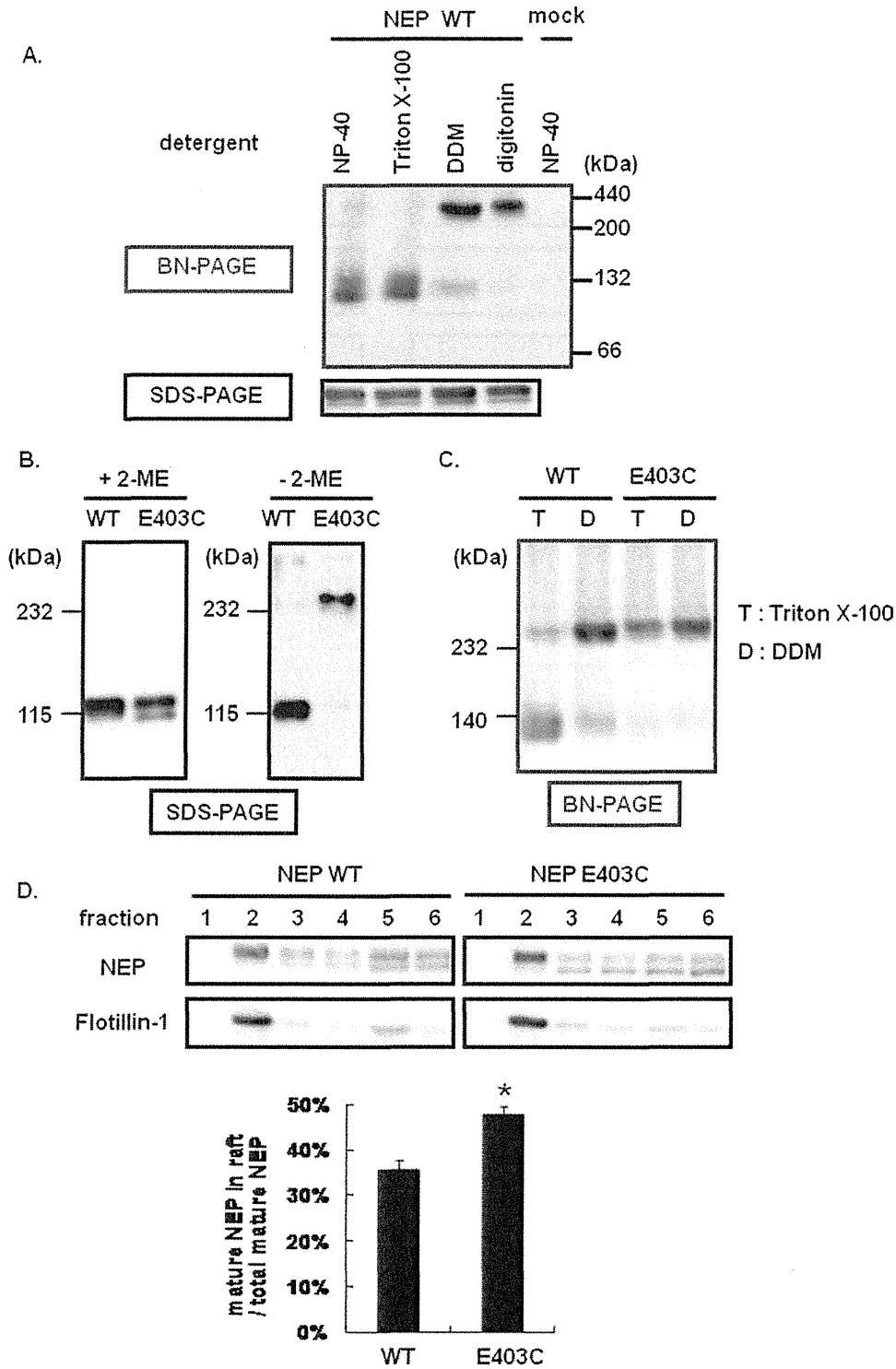

Fig. 4. Dimerization and localization of human NEP E403C in lipid rafts. **A:** Membrane fractions prepared from HEK293 cells overexpressing FLAG-NEP WT (NEP WT) or vector (mock) were dissolved in buffer containing detergents, such as NP-40, Triton X-100, DDM, and digitonin (all at a concentration of 1%). NEP complexes were analyzed by Blue Native-PAGE (BN-PAGE) or SDS-PAGE, followed by Western blotting with an anti-FLAG antibody. **B:** Membrane fractions obtained from HEK293 cells overexpressing FLAG-NEP WT (WT) or FLAG-NEP E403C (E403C) were analyzed by SDS-PAGE, performed with (**left**) or without (**right**) 2-ME. **C:** Membrane fractions obtained from HEK293 cells overexpressing FLAG-NEP WT (WT) or FLAG-NEP E403C (E403C) were dissolved in buffer containing 1% Triton X-100 (T) or 1% of DDM (D). The resulting lysates were analyzed by Blue Native-PAGE (BN-PAGE) and Western blotting with an anti-FLAG antibody. **D:** Effect of the E403C mutation on the distribution of NEP in lipid rafts. Lipid rafts from HEK293 cells overexpressing FLAG-NEP WT (NEP WT) or FLAG-NEP E403C (NEP E403C) were fractionated by sucrose density-gradient centrifugation and analyzed by Western blotting with an anti-FLAG antibody. The ratio of the amount of mature NEP localized in lipid rafts to the total amount of mature NEP was determined by densitometric measurement of protein bands corresponding to the mature form of NEP. Values represent the mean ± SD of three experiments. Statistical analysis was performed using a two-tailed Student's *t*-test. $*P < 0.05$ was considered to indicate statistical significance (bottom graph).

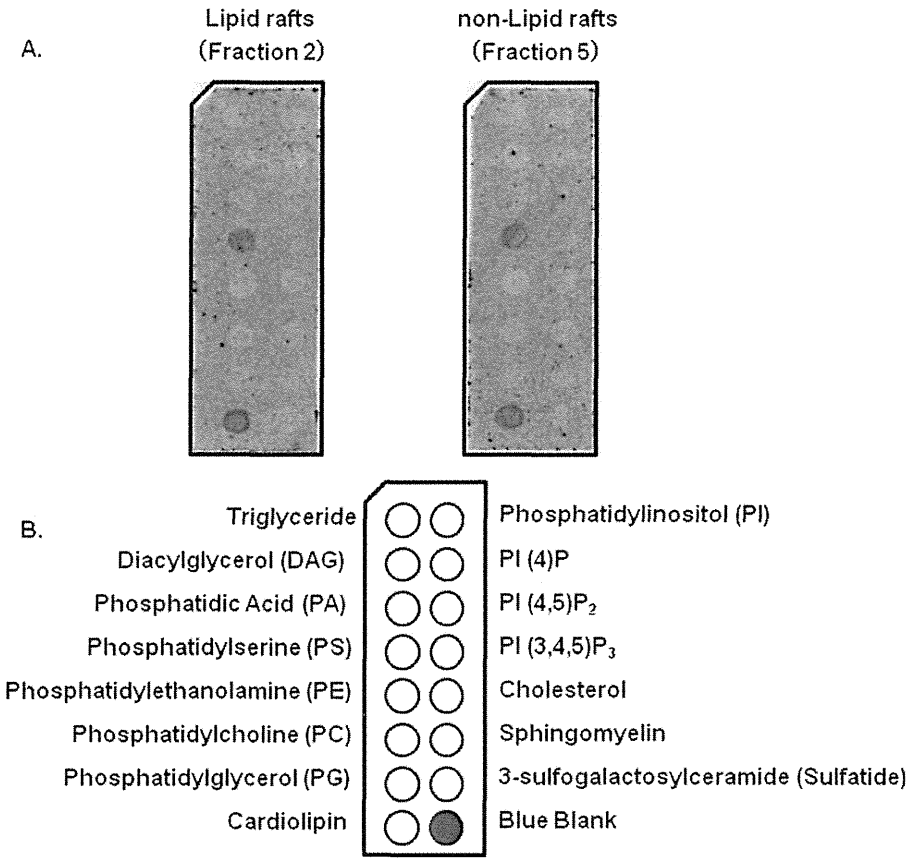

Fig. 5. Interaction of NEP with various lipids. Lipid-attached membrane was treated with sucrose density fractions of SH-SY5Y neuronal cells. After incubation and washing, the membrane was incubated with anti-NEP monoclonal antibody as described in Materials and Methods. The bound NEP was detected by ECL advance. **A:** ECL results. **B:** Lipids attached to the membrane.

Direct Inteaction of NEP With Lipids

The results described above suggest that NEP is localized in lipid rafts, possibly by its direct association with cholesterol. Finally, interaction of NEP with lipids was investigated by using lipid-spotted P-6002 membrane. Fractionated rafts (fraction 2 in Fig. 1A) and nonrafts fractions (fraction 5 in Fig. 1A) were concentrated by ultracentrifugation and incubated with lipids. After washing of the P-6002 membrane, lipid-bound NEP was detected by the specific antibody. Unexpectedly, NEP both in lipid rafts and in nonrafts fractions interacted with phosphatidylserine and cardiolipin but not with cholesterol (Fig. 5).

DISCUSSION

In this study, we found that only the mature form of NEP, glycosylated in the Golgi, and not the immature form, residing in the ER, was localized in lipid rafts (Fig. 1A,B). This indicates that complete glycosylation is required for the association of NEP with lipid rafts. Two possible explanations for this were considered. One is that maturation may be necessary for NEP to bind to a carrier protein such as a glycosylphosphatidylinositol (GPI)-anchored protein. The other is that a small conformational change caused by maturation increases the affinity of NEP for molecules found in lipid rafts, such as sphingolipids and cholesterol. With regard to the former, there have been several reports concerning carrier proteins. One study found that, when the transmembrane and C-terminal domains of BACE1 were replaced with a GPI anchor signal sequence, it was translocated to lipid rafts (Cordy et al., 2003). Another study found that the addition of the N-terminal domain of growth-associated protein 43 (GAP43) to the N-terminus of NEP increased the amount of NEP present in lipid rafts by 1.3-fold (Hama et al., 2004). With regard to the latter possible explanation, we found evidence that the localization of the mature form of NEP in lipid rafts was dependent on the content of cholesterol (Figs. 2, 3). Interestingly, although NEP was completely delocalized by cholesterol depletion, flotillin-1, a lipid raft marker, was not delocalized from lipid rafts by treatment with MβCD (Fig. 2). In this regard, flotillin-1 has been reported to be enriched in detergent-resistant microdomains that are MβCD resistant, although the mechanism

remains to be investigated (Rajendran et al., 2003). Moreover, to examine whether the delocalization of NEP from lipid rafts was caused by its direct association with cholesterol, we extracted lipid raft membranes and treated them with MβCD in vitro (Fig. 3). Consistently with the results presented in Figure 2, NEP was delocalized from lipid rafts membrane by cholesterol depletion, although not completely so (Fig. 3). The difference in the efficiency of NEP delocalization between cell and cell-free systems may be caused by the different conditions used (reaction temperature, membrane state, effects of ultracentrifugation). We conclude that the localization of mature NEP in lipid rafts depends on their cholesterol content.

We investigated the direct association of NEP with pure phospholipids and cholesterol (Fig. 5). Both NEP in rafts and nonrafts directly interacted with phosphatidylserine and cardiolipin. Cardiolipin is a major phospholipid of inner membrane of mammalian mitochondria, so phosphatidylserine might be the major interactor of NEP in lipid rafts. Moreover, immunocytochemical analysis showed that the clustered localization of endogenous NEP in SH-SY5Y cells became dispersed after MβCD treatment (Supp. Info. Fig. 1). Therefore, we conclude that NEP directly associated with phosphatidylserine in cholesterol-rich lipid rafts and MβCD-induced cholesterol depletion triggers the destruction of lipid composition and releases the NEP from rafts. However, the protease activities of mature NEP were unexpectedly comparable in lipid raft and nonlipid raft fractions, as assessed by *p*-NA peptide assay. It is possible that the fractionated lipid rafts did not reflect intracellular conditions (Pike, 2004). However, this result suggests that the association with lipid rafts does not itself modify the protease activity of NEP.

Considering the localization of Aβ in lipid rafts through association with cholesterol (Kakio et al., 2002), we hypothesized that the localization of mature NEP in lipid rafts facilitated its association with Aβ and thereby altered Aβ degradation. Recent studies have shown that lipid raft-dependent endocytosis is the predominant Aβ uptake mechanism (Lai and McLaurin, 2011), that there are correlations between memory deficits and intracellular Aβ levels in several mouse AD models (Billings et al., 2005; Knobloch et al., 2007; Bayer and Wirths, 2008), and that intracellular Aβ level correlates with extracellular amyloid deposition (Yang et al., 2011). Thus, it seems reasonable to conclude that NEP is localized and active in lipid rafts. Indeed, NEP is detected primarily in presynapses and on or around axons in the hippocampal formation (Fukami et al., 2002), and presynaptic NEP efficiently degrades Aβ (Iwata et al., 2004). Considering these findings, together with the fact that the ϵ4 allele of apolipoprotein E (apoE) is a risk factor in nonfamilial AD (Kim et al., 2009), we suggest that cholesterol, overloaded by aging or a high-fat diet, enlarges the area occupied by lipid rafts, thereby decreasing the likelihood of NEP and Aβ coming into contact with each other. As a result, Aβ becomes more abundant, oligomerizes, and causes memory deficits. However, it should be noted that cholesterol itself is a crucial contributor to synaptic structure and function. It has been reported that brain-derived neurotrophic factor (BDNF)-dependent cholesterol biosynthesis plays an important role in synapse development (Suzuki et al., 2007). It would therefore be important to maintain normal cholesterol metabolism during AD therapy.

We further investigated the effects of dimerization on the localization of NEP in lipid rafts. We introduced the E403C mutation into human NEP for the first time. The mutation was originally discovered in rabbit NEP, in which it causes the formation of a covalent homodimer (rabbit NEP normally exists as a monomer). Our results show that human NEP E403C, like rabbit NEP E403C, forms a covalent homodimer. In contrast, human NEP WT, like porcine NEP WT (Kenny et al., 1983), forms a noncovalent homodimer (Fig. 4A,B). Moreover, the noncovalent human NEP WT homodimer, though not resistant to NP-40 or Triton X-100, was resistant to DDM and digitonin. DDM and digitonin dissolve proteins modestly, so the complex remained intact after treatment with these detergents. Interestingly, the localization of mature NEP to lipid rafts was enhanced by its homodimerization (Fig. 4D). With regard to the endopeptidase activity of NEP E403C, Vmax/Km for this mutant was decreased by 50% compared with that for wild-type by using either [D-Ala^2, Leu^5] enkephalin or Suc-Ala-Ala-Leu-NH-Np as a substrate (Hoang et al., 1997). Although the NEP E403C mutant seems to be artificial and to have no physiological significance, these results imply that the protease activity of NEP might be modulated by its dimerization.

In conclusion, we have shown that cholesterol regulates the localization of mature NEP in lipid rafts, where its substrate, Aβ, accumulates. Cholesterol does not, however, modulate the protease activity of NEP.

ACKNOWLEDGMENTS

We thank Dr. Nobuhisa Iwata (Nagasaki University) for providing the protocol for the assay of neprilysin-dependent neutral endopeptidase activity.

REFERENCES

Angelisova P, Drbal K, Horejsi V, Cerny J. 1999. Association of CD10/neutral endopeptidase 24.11 with membrane microdomains rich in glycosylphosphatidylinositol-anchored proteins and Lyn kinase. Blood 93:1437–1439.

Bayer TA, Wirths O. 2008. Review on the APP/PS1KI mouse model: intraneuronal Abeta accumulation triggers axonopathy, neuron loss and working memory impairment. Genes Brain Behav 7(Suppl 1):6–11.

Billings LM, Oddo S, Green KN, McGaugh JL, LaFerla FM. 2005. Intraneuronal Abeta causes the onset of early Alzheimer's disease-related cognitive deficits in transgenic mice. Neuron 45:675–688.

Cordy JM, Hussain I, Dingwall C, Hooper NM, Turner AJ. 2003. Exclusively targeting beta-secretase to lipid rafts by GPI-anchor addition up-regulates beta-site processing of the amyloid precursor protein. Proc Natl Acad Sci U S A 100:11735–11740.

Fukami S, Watanabe K, Iwata N, Haraoka J, Lu B, Gerard NP, Gerard C, Fraser P, Westaway D, St. George-Hyslop P, Saido TC. 2002.

Abeta-degrading endopeptidase, neprilysin, in mouse brain: synaptic and axonal localization inversely correlating with Abeta pathology. Neuroscience research 43:39–56.

Hama E, Shirotani K, Iwata N, Saido TC. 2004. Effects of neprilysin chimeric proteins targeted to subcellular compartments on amyloid beta peptide clearance in primary neurons. J Biol Chem 279:30259–30264.

Hardy JA, Higgins GA. 1992. Alzheimer's disease: the amyloid cascade hypothesis. Science 256:184–185.

Hellstrom-Lindahl E, Ravid R, Nordberg A. 2008. Age-dependent decline of neprilysin in Alzheimer's disease and normal brain: inverse correlation with A beta levels. Neurobiol Aging 29:210–221.

Hoang MV, Sansom CE, Turner AJ. 1997. Mutagenesis of Glu403 to Cys in rabbit neutral endopeptidase-24.11 (neprilysin) creates a disulphide-linked homodimer: analogy with endothelin-converting enzyme. Biochem J 327:925–929.

Iwata N, Tsubuki S, Takaki Y, Shirotani K, Lu B, Gerard NP, Gerard C, Hama E, Lee HJ, Saido TC. 2001. Metabolic regulation of brain Abeta by neprilysin. Science 292:1550–1552.

Iwata N, Takaki Y, Fukami S, Tsubuki S, Saido TC. 2002. Region-specific reduction of A beta-degrading endopeptidase, neprilysin, in mouse hippocampus upon aging. J Neurosci Res 70:493–500.

Iwata N, Mizukami H, Shirotani K, Takaki Y, Muramatsu S, Lu B, Gerard NP, Gerard C, Ozawa K, Saido TC. 2004. Presynaptic localization of neprilysin contributes to efficient clearance of amyloid-beta peptide in mouse brain. J Neurosci 24:991–998.

Kakio A, Nishimoto S, Yanagisawa K, Kozutsumi Y, Matsuzaki K. 2002. Interactions of amyloid beta-protein with various gangliosides in raft-like membranes: importance of GM1 ganglioside-bound form as an endogenous seed for Alzheimer amyloid. Biochemistry 41:7385–7390.

Kanemitsu H, Tomiyama T, Mori H. 2003. Human neprilysin is capable of degrading amyloid beta peptide not only in the monomeric form but also the pathological oligomeric form. Neurosci Lett 350:113–116.

Kawarabayashi T, Shoji M, Younkin LH, Wen-Lang L, Dickson DW, Murakami T, Matsubara E, Abe K, Ashe KH, Younkin SG. 2004. Dimeric amyloid beta protein rapidly accumulates in lipid rafts followed by apolipoprotein E and phosphorylated tau accumulation in the Tg2576 mouse model of Alzheimer's disease. J Neurosci 24:3801–3809.

Kenny AJ, Fulcher IS, McGill KA, Kershaw D. 1983. Proteins of the kidney microvillar membrane. Reconstitution of endopeptidase in liposomes shows that it is a short-stalked protein. Biochem J 211:755–762.

Kim J, Basak JM, Holtzman DM. 2009. The role of apolipoprotein E in Alzheimer's disease. Neuron 63:287–303.

Knobloch M, Konietzko U, Krebs DC, Nitsch RM. 2007. Intracellular Abeta and cognitive deficits precede beta-amyloid deposition in transgenic arcAbeta mice. Neurobiol Aging 28:1297–1306.

Kojro E, Gimpl G, Lammich S, Marz W, Fahrenholz F. 2001. Low cholesterol stimulates the nonamyloidogenic pathway by its effect on the alpha-secretase ADAM 10. Proc Natl Acad Sci U S A 98:5815–5820.

Lafrance MH, Vezina C, Wang Q, Boileau G, Crine P, Lemay G. 1994. Role of glycosylation in transport and enzymic activity of neutral endopeptidase-24.11. Biochem J 302:451–454.

Lai AY, McLaurin J. 2011. Mechanisms of amyloid-beta peptide uptake by neurons: the role of lipid rafts and lipid raft-associated proteins. Int J Alzheimers Dis 2011:548380.

Matsuzaki K, Noguch T, Wakabayashi M, Ikeda K, Okada T, Ohashi Y, Hoshino M, Naiki H. 2007. Inhibitors of amyloid beta-protein aggregation mediated by GM1-containing raft-like membranes. Biochim Biophys Acta 1768:122–130.

Pike LJ. 2004. Lipid rafts: heterogeneity on the high seas. Biochem J 378:281–292.

Pike LJ. 2006. Rafts defined: a report on the Keystone Symposium on Lipid Rafts and Cell Function. J Lipid Res 47:1597–1598.

Rajendran L, Masilamani M, Solomon S, Tikkanen R, Stuermer CA, Plattner H, Illges H. 2003. Asymmetric localization of flotillins/reggies in preassembled platforms confers inherent polarity to hematopoietic cells. Proc Natl Acad Sci U S A 100:8241–8246.

Riemann D, Hansen GH, Niels-Christiansen L, Thorsen E, Immerdal L, Santos AN, Kehlen A, Langner J, Danielsen EM. 2001. Caveolae/lipid rafts in fibroblast-like synoviocytes: ectopeptidase-rich membrane microdomains. Biochem J 354:47–55.

Selkoe DJ. 2002. Alzheimer's disease is a synaptic failure. Science 298:789–791.

Suzuki S, Kiyosue K, Hazama S, Ogura A, Kashihara M, Hara T, Koshimizu H, Kojima M. 2007. Brain-derived neurotrophic factor regulates cholesterol metabolism for synapse development. J Neurosci 27:6417–6427.

von Tresckow B, Kallen KJ, von Strandmann EP, Borchmann P, Lange H, Engert A, Hansen HP. 2004. Depletion of cellular cholesterol and lipid rafts increases shedding of CD30. J Immunol 172:4324–4331.

Wada S, Morishima-Kawashima M, Qi Y, Misono H, Shimada Y, Ohno-Iwashita Y, Ihara Y. 2003. Gamma-secretase activity is present in rafts but is not cholesterol-dependent. Biochemistry 42:13977–13986.

Yang DS, Stavrides P, Mohan PS, Kaushik S, Kumar A, Ohno M, Schmidt SD, Wesson D, Bandyopadhyay U, Jiang Y, Pawlik M, Peterhoff CM, Yang AJ, Wilson DA, St. George-Hyslop P, Westaway D, Mathews PM, Levy E, Cuervo AM, Nixon RA. 2011. Reversal of autophagy dysfunction in the TgCRND8 mouse model of Alzheimer's disease ameliorates amyloid pathologies and memory deficits. Brain 134:258–277.

Biochemical and Biophysical Research Communications 417 (2012) 462–467

Contents lists available at SciVerse ScienceDirect

Biochemical and Biophysical Research Communications

journal homepage: www.elsevier.com/locate/ybbrc

Tumor suppressor cell adhesion molecule 1 (CADM1) is cleaved by a disintegrin and metalloprotease 10 (ADAM10) and subsequently cleaved by γ-secretase complex

Yusuke Nagara [a], Man Hagiyama [b,c], Naoya Hatano [d], Eugene Futai [a,1], Satoshi Suo [a], Yutaka Takaoka [e], Yoshinori Murakami [b], Akihiko Ito [b,c,*], Shoichi Ishiura [a]

[a] Department of Life Sciences, Graduate School of Arts and Sciences, The University of Tokyo, 3-8-1 Komaba, Meguro-ku, Tokyo 153-8902, Japan
[b] The Division of Molecular Pathology, Institute of Medical Science, The University of Tokyo, 4-6-1 Shirokanedai, Minato-ku, Tokyo 108-8639, Japan
[c] Department of Pathology, Faculty of Medicine, Kinki University, 377-2 Ohno-Higashi, Osaka-Sayama, Osaka 589-8511, Japan
[d] The Integrated Center for Mass Spectrometry, Kobe University Graduate School of Medicine, 7-5-1 Kusunoki-cho, Chuo-ku, Kobe 650-0017, Japan
[e] Division of Medical Informatics and Bioinformatics, Kobe University Hospital, 7-5-2 Kusunoki-cho, Chuo-ku, Kobe 650-0017, Japan

ARTICLE INFO

Article history:
Received 21 November 2011
Available online 7 December 2011

Keywords:
CADM1
ADAM10
γ-Secretase
Shedding
RIP
Tumor suppressor gene

ABSTRACT

Cell adhesion molecule 1 (CADM1) is a type I transmembrane glycoprotein expressed in various tissues. CADM1 is a cell adhesion molecule with many functions, including roles in tumor suppression, apoptosis, mast cell survival, synapse formation, and spermatogenesis. CADM1 undergoes membrane-proximal cleavage called shedding, but the sheddase and mechanisms of CADM1 proteolysis have not been reported. We determined the cleavage site involved in CADM1 shedding by LC/MS/MS and showed that CADM1 shedding occurred in the membrane fraction and was inhibited by tumor necrosis factor-α protease inhibitor-1 (TAPI-1). An siRNA experiment revealed that ADAM10 mediates endogenous CADM1 shedding. In addition, the membrane-bound fragment generated by shedding was further cleaved by γ-secretase and generated CADM1-intracellular domain (ICD) in a mechanism called regulated intramembrane proteolysis (RIP). These results clarify the detailed mechanism of membrane-proximal cleavage of CADM1, suggesting the possibility of RIP-mediated CADM1 signaling.

1. Introduction

Cell adhesion molecule 1 (CADM1) is a 100–120-kDa multifunctional cell adhesion molecule. CADM1 is a member of the immunoglobulin superfamily and is a type I transmembrane glycoprotein. The extracellular domain of CADM1 undergoes homophilic or heterophilic interaction with necl-1, nectin-3, and CRTAM (class-I MHC-restricted T cell-associated molecule) [1], whereas the intracellular domain interacts with DAL-1 via its band 4.1 binding domain [2] and with pals2 [3] and MPP3 [4] via its PDZ binding domain. CADM1 is expressed in various tissues and organs, including the brain, mast cells, testis, and lung [5].

Recently, Tanabe et al. reported that CADM1 undergoes juxtamembrane cleavage in neurons [6]. We reported previously that shedding fragments were found from mast cells [7] and human mesothelioma samples [8]. These observations suggest that CADM1 shedding is a common event. CADM1 shedding seems to regulate adhesion between mesothelial and mesothelioma cells by down-regulating full-length CADM1, thereby regulating the growth and scattering of mesothelioma cells [8]. Tanabe et al. reported that certain isoforms of CADM1 produce a 20-kDa C-terminal fragment and that production of this fragment is inhibited by the broad-spectrum metalloprotease inhibitor TAPI-1. They concluded that CADM1 is shed by an ADAM17-like protease [6]. The ADAM family metalloproteases are the major membrane-bound sheddases, which are responsible for shedding of many membrane protein substrates. Among the family members, ADAM10 and ADAM17 are the major sheddases and have large numbers of known substrates. After shedding, some membrane proteins undergo a secondary cleavage within the membrane mediated by γ-secretase. For example, Notch, ErbB4, and amyloid precursor protein (APP) are cleaved by γ-secretase [9]. The γ-cleavage product, the intracellular domain (ICD) of the substrate, often acts as a transcriptional regulator. ICDs of Notch and other γ-secretase substrates, such as CD44 [10] and APP [11], act as nuclear signaling molecules that regulate gene expression.

In this study, we focused on CADM1 proteolysis. The aim of this study was to characterize the sheddase of CADM1 and to examine proteolysis events occurring on the CADM1 molecule. Our results

* Corresponding author at: Department of Pathology, Faculty of Medicine, Kinki University, 377-2 Ohno-Higashi, Osaka-Sayama, Osaka 589-8511, Japan. Fax: +81 72 360 2028.
E-mail address: aito@med.kindai.ac.jp (A. Ito).
[1] Present address: Department of Molecular Cell Science, Graduate School of Agricultural Science, Tohoku University, 1-1 Tsutsumidori Amamiya-machi, Aoba-ku, Sendai, Miyagi 981-8555, Japan.

0006-291X/$ - see front matter © 2011 Elsevier Inc. All rights reserved.
doi:10.1016/j.bbrc.2011.11.140

indicated that CADM1 shedding is catalyzed by a protease associated with the cell membrane, and ADAM10 endogenously sheds CADM1. Furthermore, we discovered γ-cleavage of CADM1, which is catalyzed by γ-secretase. These results provide a possible signal-transduction mechanism involving regulated intramembrane proteolysis (RIP).

2. Materials and methods

2.1. Reagents and antibodies

TAPI-1, *N*-[*N*-(3,5-difluorophenacetyl-L-alanyl)]-(*S*)-phenylglycine t-butyl ester (DAPT), and L-685,458 were purchased from Calbiochem (San Diego, CA). Phorbol-12-myristate-13-acetate (PMA) was purchased from Wako (Osaka, Japan). Phenylmethylsulfonyl fluoride (PMSF) and protease inhibitor cocktail (cat.# P8340) were purchased from Sigma (St. Louis, MO).

Anti-CADM1-cyto antibody was generated according to the method described by Wakayama et al. [12]. This antibody recognizes the C-terminal 20 amino acids of CADM1. Anti-CADM1-ecto antibody (3E1) is our original as described previously [13]. This antibody recognizes 2nd Ig domain in the ectodomain. Peroxidase-conjugated secondary antibodies were purchased from Cell Signaling Technology (Danvers, MA).

2.2. In vitro assay of CADM1 shedding

Confluent HEK293 cells were harvested and homogenized in buffer P (20 mM PIPES-KOH pH 7.0, 140 mM KCl, 250 mM sucrose) at 4 °C. The homogenized cells were centrifuged at 800*g* for 10 min to remove the nuclei and cell debris. The supernatant was then ultracentrifuged at 100,000*g* for 1 h, and the resulting pellet was washed with buffer P and ultracentrifuged again at 100,000*g* for 1 h. The resulting pellet (the membrane fraction) was resuspended in buffer P and stored at −80 °C until use.

This membrane fraction was incubated at 37 °C for 1.5 h with the indicated concentrations of protease inhibitors or vehicle only (DMSO, 0.2% for TAPI-1, 1% for PMSF and protease inhibitor cocktail), and the reaction was stopped by addition of 2× sample buffer and boiling for 5 min. These samples were subjected to Western blotting analysis using anti-CADM1-cyto antibody.

2.3. Western blotting analysis

SDS–PAGE and Western blotting were performed according to the standard reducing SDS–PAGE and Western blotting protocols. For detection of CADM1-ICD, samples were separated by Tris–tricine SDS–PAGE and transferred onto Immobilon-P membranes (Millipore, Billerica, MA). The membranes were boiled in PBS for 5 min after transfer and then subjected to blocking, antibody treatments, and subsequent procedures.

2.4. Transfection of siRNA and expression vectors

siRNA (Stealth Select RNAi) specific for human ADAM10 (HSS100167), ADAM17 (HSS110435), and control siRNA (Stealth RNAi negative control low GC duplex, 12935-200) were purchased from Invitrogen (Carlsbad, CA). Saos-2 cells at 40–50% confluence were transfected with siRNAs using Lipofectamine RNAiMax Transfection Reagent (Invitrogen) according to the manufacturer's instructions. After 96 h of incubation, cells were harvested, and the cell lysates were analyzed by Western blotting.

2.5. Cell culture

cDNA encoding mouse-CADM1 (GenBank ID: AB052293) was cloned into the expression vector pCX4-bsr and confirmed by DNA sequencing (pCX4bsr-CADM1) [7]. COS7 cells and NIH3T3 cells were transfected with the pCX4bsr-CADM1 vector, and blasticidin-resistant cells were selected by continuing the culture in the presence of blasticidin (3 μg/mL) for 4 weeks (COS7-mCADM1 and NIH3T3-mCADM1). MEF and nicastrin$^{-/-}$ MEF cells were kind gifts from Dr. Philip C. Wong (The Johns Hopkins University), and presenilin 1/2 double knockout MEF was a kind gift from Dr. Bart De Strooper (Vlaams Instituut voor Biotechnologie). These cells, HEK293, and human osteosarcoma Saos-2 were maintained in DMEM supplemented with 10% fetal bovine serum and penicillin/streptomycin. In γ-secretase inhibitor assay, confluent COS7-mCADM1 cells were treated with 200 ng/mL PMA for 2 h, and then γ-secretase inhibitor (1 μM DAPT or 1 μM L-685,458) or vehicle (DMSO) was added. After incubation for the indicated times, cells were harvested, and the cell lysates were analyzed by Western blotting.

2.6. Mass spectrometric analysis

NIH3T3-mCADM1 cells were harvested, and the membrane fraction extract was prepared using Subcellular Proteome Extraction Kit (Merck, Whitehouse Station, NJ). The membrane fraction extract was concentrated using Amicon Ultra 15 (Millipore) and then immunoprecipitated using anti-CADM1cyto antibody. The precipitate was mixed with sample buffer and subjected to SDS–PAGE. The gel was stained with EZ-Blue (Sigma), and the alphaCTF band was cut out. In-gel digestion with chymotrypsin was performed according to the published methods [14,15]. The digested peptides were subjected to liquid chromatography (LC)/MS/MS analysis on a Q-Tof2 quadrupole/time-of-flight (TOF) hybrid mass spectrometer (Micromass, Manchester, UK) interfaced with a capillary reversed-phase liquid chromatography system (Micromass CapLC system) as described previously [14]. The MS/MS data were analyzed with Mascot MS/MS Ion Search (version 2.1.6; Matrix Science Ltd., London, UK) to assign the obtained peptides to the NCBI non-redundant database (NCBInr 20060718; 3784285 sequences) as described previously [14].

3. Results

3.1. CADM1 shedding is promoted by phorbol ester

To study shedding of CADM1, we first generated a stable COS7 cell line expressing murine CADM1 (COS7-mCADM1). Several CADM1-derived bands, including bands of approximately 15 and 35 kDa, were detected from COS7-mCADM1 lysate by Western blotting with an antibody that recognizes the C-terminal of CADM1. We refer to the 15- and 35-kDa fragments as alphaCTF (C-terminal fragment) and betaCTF, respectively. AlphaCTF is likely to be the same shedding fragment of CADM1 reported previously [6], and betaCTF is another fragment of CADM1. As shedding of some other membrane proteins is promoted by phorbol esters such as PMA, we examined the effects of PMA treatment on CADM1 shedding (Fig. 1A) and found that alphaCTF was increased after PMA treatment. On the other hand, no apparent changes were observed in the 35-kDa band, which was thought to be another cleaved fragment of CADM1.

We next concentrated CADM1 alphaCTF by immunoprecipitation and determined the cleavage site by LC/MS/MS. Following SDS–PAGE, the gel slice containing the alphaCTF band was excised

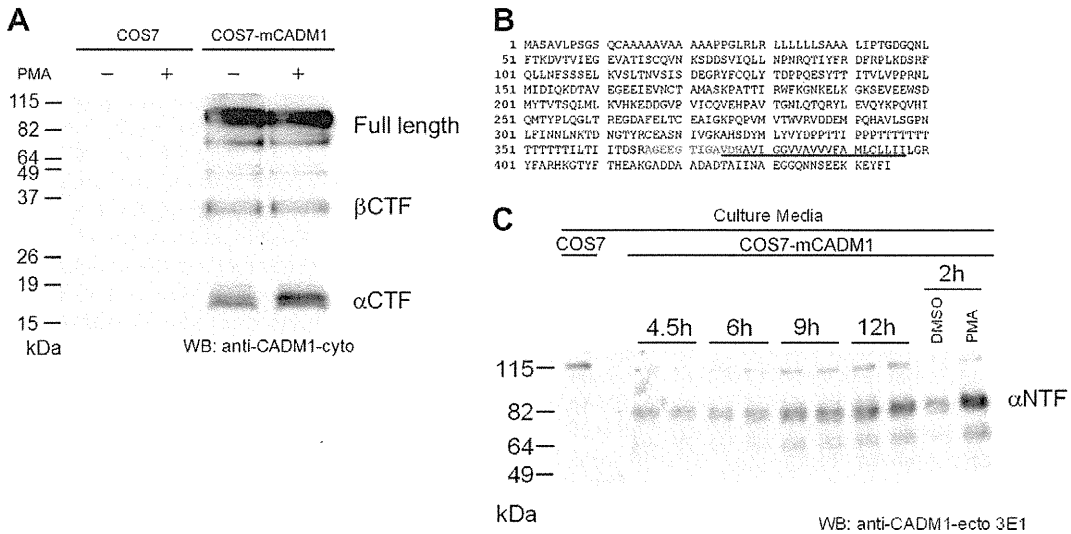

Fig. 1. Ectodomain shedding of CADM1, (A) COS7-mCADM1 cells were treated with 200 ng/mL PMA or vehicle alone for 30 min and then harvested. Cell lysates were analyzed by Western blotting using anti-CADM1-cyto antibody. (B) Determination of the cleavage site of CADM1 shedding. The peptide detected by LC/MS/MS is indicated in red, and the transmembrane region is underlined. (C) Culture medium of subconfluent COS7-mCADM1 cells was changed to serum-free medium and incubated for the indicated times (duplicate results are shown). To evaluate PMA-dependent secretion, 200 ng/mL PMA or vehicle (DMSO) was added to the serum-free medium and incubated for 2 h. The medium was then harvested and concentrated by TCA precipitation. The precipitate was analyzed by Western blotting using anti-CADM1-ecto antibody 3E1. (For interpretation of the references to color in this figure legend, the reader is referred to the web version of this article.)

and cleaved with chymotrypsin in the gel. LC/MS/MS detected a peptide fragment with an N-terminus generated by proteases other than chymotrypsin (Fig. 1B). This observation suggested that the N-terminus of the detected peptide was generated by shedding. The cleavage site was between R365 and A366, nine amino acid residues from the predicted transmembrane region in the extracellular domain. This result predicted that alphaCTF is an 80 amino acids fragment. Larger apparent molecular weight of this fragment on Western blotting is probably due to O-linked glycosylation. This result also predicted that N-terminal fragments are released into the culture medium after shedding and that PMA treatment would increase this release. Therefore, we analyzed the culture media by Western blotting and found that there was indeed a CADM1 fragment corresponding in size to NTF after cleavage that produces alphaCTF. As expected, we also found that PMA treatment increased the amount of CADM1 fragments in the culture medium (Fig. 1C).

Taken together, these results suggest that CADM1 shedding produces alphaCTF and a corresponding extracellular fragment, that cleavage occurs in the membrane-proximal region of CADM1 extracellular domain, and that shedding is promoted by PMA.

3.2. CADM1 shedding was detected in an in vitro membrane-fraction incubation assay

CADM1 shedding was previously shown to be inhibited by TAPI-1, a broad-spectrum inhibitor that targets many metalloproteases such as ADAMs and MMPs. Among them, those with transmembrane domains are known to shed a large number of transmembrane substrates.

To obtain further information about CADM1 sheddase, we performed an *in vitro* assay using total cell membrane fraction and focusing on membrane-bound proteases.

To avoid artifacts due to overexpression of CADM1, we prepared total membrane fraction from HEK293 cells, which constitutively express endogenous CADM1. The total membrane fraction prepared by ultracentrifugation was incubated. The level of alphaCTF increased after incubation, whereas that of full-length CADM1 decreased (Fig. 2A). BetaCTF was barely detectable in this preparation. The increase in the 15-kDa band was inhibited by addition of TAPI-1 (Fig. 2A and B), as reported previously by Tanabe et al. [6], who added TAPI-1 to neuronal cells. Serine, cysteine, and aspartic protease inhibitors showed no inhibitory effect on CADM1 shedding (Fig. 2C). Thus, we could reconstitute shedding of CADM1 *in vitro* by incubation of the membrane fraction and could characterize the sensitivity to protease inhibitors using this method. These results indicated that a membrane-associated metalloprotease possesses CADM1 shedding activity.

3.3. CADM1 shedding is mediated by the metalloprotease ADAM10

Many membrane molecules undergo shedding, and ADAM10 and ADAM17 were reported to be two major membrane-associated sheddases. An siRNA approach was employed here to investigate whether ADAM10 and/or ADAM17 cleaved CADM1. The Saos-2 human osteosarcoma cell line, which shows high-level expression of endogenous ADAM10, was used in this assay. The siRNAs used downregulated the mature form of targeted ADAMs as well as the proform (Fig. 3A). Knockdown of ADAM10 expression decreased the amount of alphaCTF, whereas the knockdown of ADAM17 had no effect on the amount of alphaCTF. Furthermore, ADAM10 knockdown abolished PMA-dependent accumulation of alphaCTF (Fig. 3B). These observations indicated that CADM1 is cleaved endogenously by the metalloprotease ADAM10, and PMA-dependent cleavage of CADM1 is also mainly mediated by ADAM10.

3.4. γ-Secretase-like cleavage is abrogated in the presence of γ-secretase inhibitors and in γ-secretase KO cells

Following membrane-proximal cleavage, similar to CADM1 shedding, some membrane proteins undergo a second cleavage mediated by γ-secretase. To determine whether CADM1 is cleaved by γ-secretase, we examined the effects of γ-secretase inhibition on the amounts of cleaved CADM1 fragments after induction of shedding by PMA. COS7-mCADM1 cells were treated with PMA or vehicle alone and then treated with γ-secretase inhibitor (DAPT or L-685,458) or vehicle alone. The amount of alphaCTF increased in

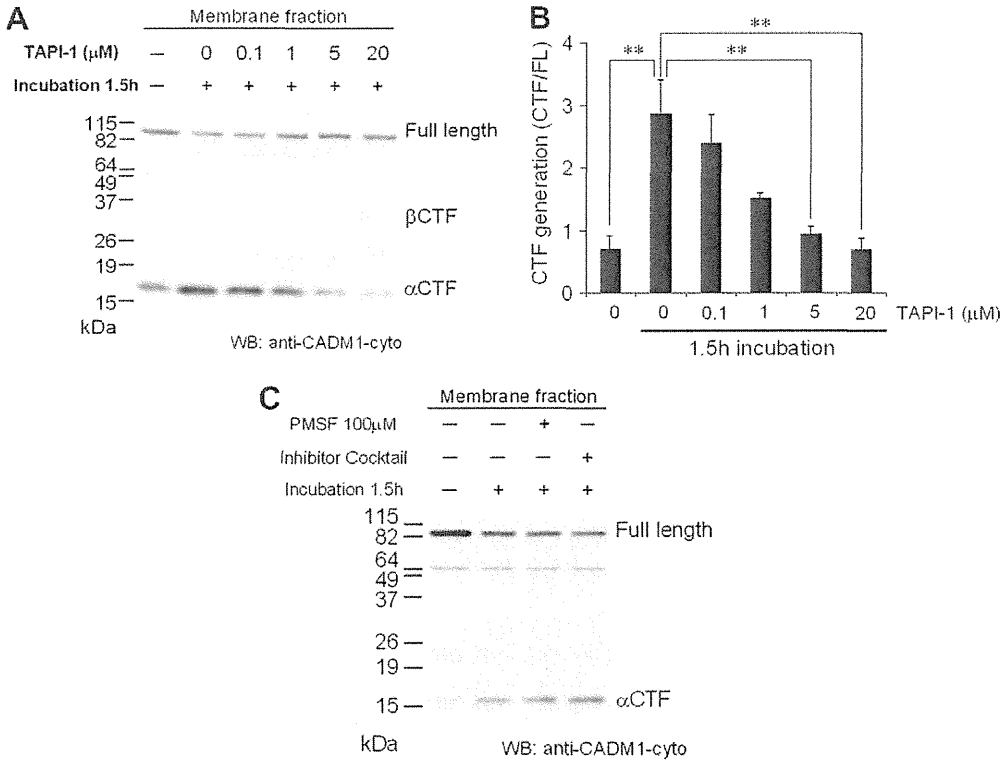

Fig. 2. *In vitro* CADM1 shedding assay. (A–C) Membrane fraction was obtained from HEK293 cells as described in Section 2. The membrane fraction was incubated with the indicated concentration of protease inhibitors and subjected to Western blotting analysis using anti-CADM1-cyto antibody. The results of densitometric analysis of CADM1-CTF generation in (A) are shown in (B). CTF generation was calculated as CTF/full-length ratio by densitometric analysis. Results were obtained from three independent experiments and are expressed as means ± SEM. Data were analyzed by one-way analysis of variance followed by Dunnett's multiple comparison test. **Statistically significant compared with "1.5 h, 0 μM TAPI-1" ($p < 0.01$). The inhibitor cocktail in (C) was from Sigma (P8340).

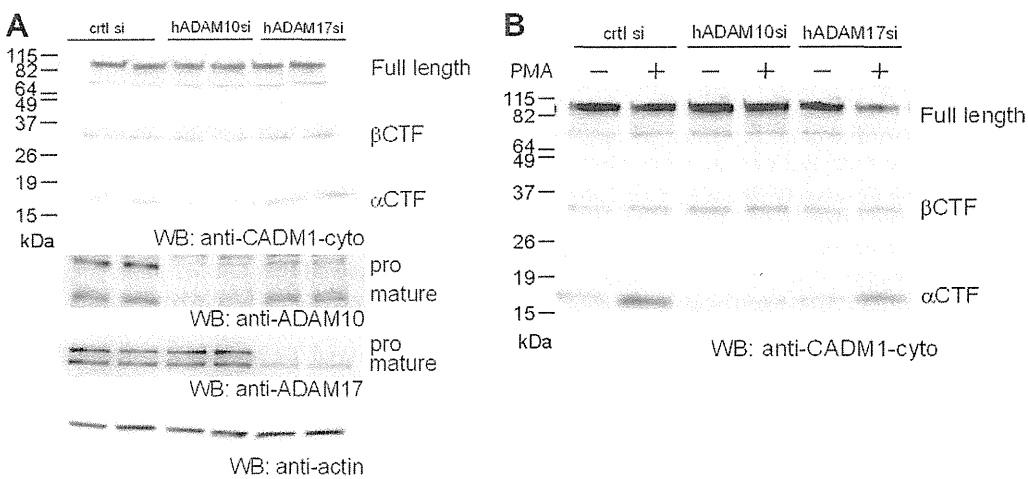

Fig. 3. Knockdown of ADAM10 decreases CADM1-CTF level. (A) Saos-2 cells were transfected with siRNAs against ADAM10 or ADAM17 or with control siRNA. Cells were harvested after 96 h of incubation. Cell lysates were subjected to Western blotting analysis using anti-CADM1-cyto antibody (duplicate results are shown). In (B), cells were treated with 200 ng/mL PMA or vehicle only (DMSO) for 4 h and then harvested.

the presence of γ-secretase inhibitor (Fig. 4A), indicating γ-secretase-dependent degradation of alphaCTF. This finding suggested that alphaCTF was cleaved by γ-secretase into a cytosolic fragment, CICD (CADM1 intracellular domain). With membrane boiling and prolonged exposure, a CADM1-derived band of nearly 6 kDa was detected (Fig. 4A). Membrane boiling contributes to the detection of this 6 kDa fragment, and it is necessary to boil the membrane for the detection of obvious CICD band. The amount of this fragment was decreased with γ-secretase inhibitor treatment, consistent with alphaCTF accumulation (Fig. 4A). γ-Secretase cleaves its substrates within the cell membrane at around three amino acids from the cytosolic end of the transmembrane region of the substrate and generates a fragment with an intact cytoplasmic domain. The theoretical molecular weight of CADM1 cytoplasmic domain is 5.3 kDa. This fragment is the cleavage product of CADM1 generated by γ-secretase. These results suggest that alphaCTF is cleaved by γ-secretase and generates CICD fragments.

We employed another approach to further confirm this possibility. γ-Secretase consists of four proteins, presenilin, nicastrin, Aph-1, and Pen-2, all of which are indispensable for its activity. We used

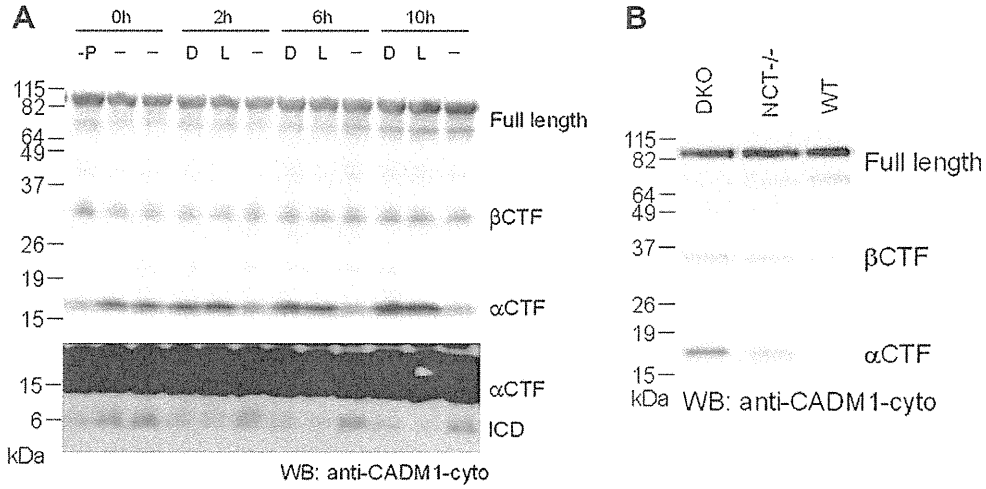

Fig. 4. CADM1-ICD generation is dependent on γ-secretase. (A) COS7-mCADM1 cells were pretreated with 200 ng/mL PMA or vehicle alone (-P: DMSO) for 2 h, and subsequently treated with γ-secretase inhibitors (D: 1 μM DAPT or L: 1 μM L-685,458) or vehicle alone (–: DMSO) and incubated for the indicated times. (B) Cultured cells of two mouse embryonic fibroblast (MEF) cell lines lacking γ-secretase activity and a wild-type MEF cell line were harvested. Cell lysates were analyzed by Western blotting using anti-CADM1-cyto antibody.

two MEF cell lines with no γ-secretase activity, one lacking presenilin-1 and presenilin-2 (PSDKO) and another lacking nicastrin ($NCT^{-/-}$) [16,17]. On Western blotting analysis, the alphaCTF level was increased in γ-secretase KO MEFs but not in wild-type MEFs (Fig. 4B). These results were consistent with those of γ-secretase inhibitor assay, indicating that alphaCTF is processed into CICD by γ-secretase.

4. Discussion

Many previous studies have addressed the various functions of CADM1. Genetic analyses of human cancer suggest that CADM1 has potent tumor-suppressor activity. CADM1 was also shown to suppress tumorigenicity in mouse models, to induce apoptosis, and to suppress cell proliferation *in vitro* [18]. However, the molecular mechanisms underlying these and other functions are largely unknown. In the present study, we focused on membrane protein proteolysis, which may modulate or mediate the functions of such proteins. A previous study indicated that certain CADM1 isoforms are shed due to the action of a ADAM17-like protease [6]. We examined CADM1 proteolysis in more detail, and here we demonstrated the two-step mechanism of CADM1 proteolysis including shedding and RIP with identification of the cleavage site of shedding, sheddase, and subsequent γ-cleavage.

We first demonstrated enhancement of CADM1 shedding by PMA and accumulation of the cleaved extracellular fragment in the medium. A soluble CADM1 isoform was shown to elicit directional neurite extension up a CADM1 concentration gradient [19]. According to the cleavage site determined here, the whole sequence of the soluble isoform was contained within the shed fragment with the exception of two amino acids near the isoform-specific C-terminus. These observations suggest that CADM1 extracellular fragment may also serve as a neurite attractant with a regulated mechanism of secretion. Unexpectedly, although betaCTF was abundant in several cell lines, betaNTF was much less abundant than alphaNTF in the culture medium of the same cells. An as-yet-unknown cellular system may retain and degrade the "extracellular" fragment within the cells.

We developed an *in vitro* shedding assay and demonstrated that CADM1 shedding could occur not only in the intact cell but also in the isolated membrane fraction. This method can be used as a novel *in vitro* assay for ectodomain shedding. To date, *in vitro* shedding assays have mostly been performed by the addition of purified protease to the membrane fraction, which contains the substrate. Our method is closer to physiological conditions because the endogenous localization of a protease and its substrate should be intact. Using this method, we showed here that shedding of CADM1 was directly mediated by a membrane-bound metalloprotease. TAPI-1 was also shown to have an inhibitory effect on CADM1 shedding, consistent with previous findings [6]. Furthermore, the results of siRNA experiments indicated that ADAM10, but not ADAM17, is a potent endogenous sheddase of CADM1. In contrast, previous studies showed that nectin-1 and nectin-4, both of which are adhesion molecules related to CADM1, are cleaved by ADAM10 and ADAM17, respectively [20,21]. ADAM10 is a well-known sheddase that cleaves many other adhesion molecules. Although no consensus cleavage sequence is known for ADAM10, this molecule cleaves its substrate at a site 8–20 amino acids from the transmembrane region in its ectodomain [22]. In the present study, the cleavage site for CADM1 shedding was determined to be nine amino acids from the transmembrane region by MS analysis, indicating that shedding of CADM1 is similar to that of other known cell-surface molecules mediated by ADAM10.

We next showed that CADM1 undergoes γ-secretase-mediated cleavage and generates CADM1-ICD using inhibitors or γ-secretase-deficient cell lines. A previous study indicated that nectin-1α is also cleaved by γ-secretase-like activity to generate ICD [23]. This process is known to involve proteolytic cleavage called RIP, in which removal of the ectodomain by shedding is necessary for the second cleavage catalyzed by γ-secretase [9]. Our data suggested that the substrate of γ-cleavage is the membrane-bound shedding product alphaCTF, consistent with the known mechanism of RIP. Compared with alphaCTF, the amount of CICD fragment is very small, and the difference between the amount of the fragment with and without inhibitor treatment was small. This is probably because of the rapid degradation of CICD, as many other ICD fragments generated by γ-secretase, including Notch ICD, are known to be rapidly degraded in a proteasome-dependent manner [23].

ICD often acts as a signal transducer. Nuclear staining for CADM1 was observed on microscopic analysis using C-terminal GFP-tagged CADM1 or antibody against CADM1 cytosolic domain ([1] and unpublished data). CASK, a protein that binds to CADM1 cytoplasmic domain, is partially localized to the nucleus and interacts with the T-box transcription factor Tbr-1, inducing transcription of genes including NR2b [24]. CADM1-ICD may be transported into the nucleus together with CASK and may modulate

target genes of the Tbr-1-CASK complex. These observations suggest that CADM1 may function in the nucleus as a signal transducer via RIP.

CADM1 is known to act as a tumor suppressor in nude mice, and its expression is reduced in many types of human tumor. ADAM10 is overexpressed in colorectal cancer [25]. The hypermethylation of CADM1 and the reduced expression of CADM1 protein in colorectal cancer have also been reported [26]. ADAM10-mediated shedding may be a mechanism involved in the downregulation of CADM1 in colorectal cancer, which leads to disruption of CADM1-mediated tumor suppression. On the other hand, the functional significance of γ-cleavage is rather complicated. CADM1-ICD has two protein-binding domains, band 4.1 binding domain and PDZ binding domain [1]. These domains are indispensable for the tumor-suppressive functions of CADM1, including tumor suppression in mice, the induction of apoptosis, and the suppression of epithelial-mesenchymal transition [27–29], suggesting the functional significance of the CADM1 cytoplasmic domain.

In conclusion, our data demonstrated that CADM1 cleavage is mediated by ADAM10 and γ-secretase. This mechanism may be important for the downregulation of CADM1 by proteolytic degradation or for tumor-suppressive activity and other functions of CADM1, probably through the activation of CADM1-ICD and reduction of cell–cell adhesion.

Acknowledgments

We thank Dr. Bart De Strooper (Vlaams Instituut voor Biotechnologie) for Presenilin 1/2 double knockout cells and Dr. Philip C. Wong (The Johns Hopkins University) for Nicastrin$^{-/-}$ cells. Y.N. is supported by a JSPS Research Fellowship for Young Scientists.

References

[1] M. Masuda, M. Yageta, H. Fukuhara, et al., The tumor suppressor protein TSLC1 is involved in cell-cell adhesion, J. Biol. Chem. 277 (2002) 31014–31019.
[2] M. Yageta, M. Kuramochi, M. Masuda, et al., Direct association of TSLC1 and DAL-1, two distinct tumor suppressor proteins in lung cancer, Cancer Res. 62 (2002) 5129–5133.
[3] T. Shingai, W. Ikeda, S. Kakunaga, et al., Implications of nectin-like molecule-2/IGSF4/RA175/SgIGSF/TSLC1/SynCAM1 in cell–cell adhesion and transmembrane protein localization in epithelial cells, J. Biol. Chem. 278 (2003) 35421–35427.
[4] H. Fukuhara, M. Masuda, M. Yageta, et al., Association of a lung tumor suppressor TSLC1 with MPP3, a human homologue of Drosophila tumor suppressor Dlg, Dlg. Oncogene 22 (2003) 6160–6165.
[5] Y. Koma, A. Ito, T. Wakayama, et al., Cloning of a soluble isoform of the SgIGSF adhesion molecule that binds the extracellular domain of the membrane-bound isoform, Oncogene 23 (2004) 5687–5692.
[6] Y. Tanabe, T. Kasahara, T. Momoi, et al., Neuronal RA175/SynCAM1 isoforms are processed by tumor necrosis factor-alpha-converting enzyme (TACE)/ADAM17-like proteases, Neurosci. Lett. 444 (2008) 16–21.
[7] A. Ito, T. Jippo, T. Wakayama, et al., SgIGSF: a new mast-cell adhesion molecule used for attachment to fibroblasts and transcriptionally regulated by MITF, Blood 101 (2003) 2601–2608.
[8] A. Ito, M. Hagiyama, T. Mimura, et al., Expression of cell adhesion molecule 1 in malignant pleural mesothelioma as a cause of efficient adhesion and growth on mesothelium, Lab. Invest. 88 (2008) 504–514.
[9] J.O. Ebinu, B.A. Yankner, A RIP tide in neuronal signal transduction, Neuron 34 (2002) 499–502.
[10] I. Okamoto, Y. Kawano, D. Murakami, et al., Proteolytic release of CD44 intracellular domain and its role in the CD44 signaling pathway, J. Cell Biol. 155 (2001) 755–762.
[11] W.T. Kimberly, J.B. Zheng, S.Y. Guenette, et al., The intracellular domain of the beta-amyloid precursor protein is stabilized by Fe65 and translocates to the nucleus in a notch-like manner, J. Biol. Chem. 276 (2001) 40288–40292.
[12] T. Wakayama, H. Koami, H. Ariga, et al., Expression and functional characterization of the adhesion molecule spermatogenic immunoglobulin superfamily in the mouse testis, Biol. Reprod. 68 (2003) 1755–1763.
[13] T. Furuno, A. Ito, Y. Koma, et al., The spermatogenic Ig superfamily/synaptic cell adhesion molecule mast-cell adhesion molecule promotes interaction with nerves, J. Immunol. 174 (2005) 6934–6942.
[14] A. Shevchenko, M. Wilm, O. Vorm, et al., Mass spectrometric sequencing of proteins silver-stained polyacrylamide gels, Anal. Chem. 68 (1996) 850–858.
[15] M. Kikuchi, N. Hatano, S. Yokota, et al., Proteomic analysis of rat liver peroxisome: presence of peroxisome-specific isozyme of Lon protease, J. Biol. Chem. 279 (2004) 421–428.
[16] A. Herreman, L. Serneels, W. Annaert, et al., Total inactivation of gamma-secretase activity in presenilin-deficient embryonic stem cells, Nat. Cell Biol. 2 (2000) 461–462.
[17] T. Li, G. Ma, H. Cai, et al., Nicastrin is required for assembly of presenilin/gamma-secretase complexes to mediate Notch signaling and for processing and trafficking of beta-amyloid precursor protein in mammals, J. Neurosci. 23 (2003) 3272–3277.
[18] Y. Murakami, Involvement of a cell adhesion molecule, TSLC1/IGSF4, in human oncogenesis, Cancer Sci. 96 (2005) 543–552.
[19] M. Hagiyama, N. Ichiyanagi, K.B. Kimura, et al., Expression of a soluble isoform of cell adhesion molecule 1 in the brain and its involvement in directional neurite outgrowth, Am. J. Pathol. 174 (2009) 2278–2289.
[20] J. Kim, C. Lilliehook, A. Dudak, et al., Activity-dependent alpha-cleavage of nectin-1 is mediated by a disintegrin and metalloprotease 10 (ADAM10), J. Biol. Chem. 285 (2010) 22919–22926.
[21] S. Fabre-Lafay, S. Garrido-Urbani, N. Reymond, et al., Nectin-4, a new serological breast cancer marker, is a substrate for tumor necrosis factor-alpha-converting enzyme (TACE)/ADAM-17, J. Biol. Chem. 280 (2005) 19543–19550.
[22] M.S. Rosendahl, S.C. Ko, D.L. Long, et al., Identification and characterization of a pro-tumor necrosis factor-alpha-processing enzyme from the ADAM family of zinc metalloproteases, J. Biol. Chem. 272 (1997) 24588–24593.
[23] D.Y. Kim, L.A. Ingano, D.M. Kovacs, Nectin-1alpha, an immunoglobulin-like receptor involved in the formation of synapses, is a substrate for presenilin/gamma-secretase-like cleavage, J. Biol. Chem. 277 (2002) 49976–49981.
[24] T.F. Wang, C.N. Ding, G.S. Wang, et al., Identification of Tbr-1/CASK complex target genes in neurons, J. Neurochem. 91 (2004) 1483–1492.
[25] T. Knosel, A. Emde, K. Schluns, et al., Immunoprofiles of 11 biomarkers using tissue microarrays identify prognostic subgroups in colorectal cancer, Neoplasia 7 (2005) 741–747.
[26] K. Chen, G. Wang, L. Peng, et al., CADM1/TSLC1 inactivation by promoter hypermethylation is a frequent event in colorectal carcinogenesis and correlates with late stages of the disease, Int. J. Cancer 128 (2011) 266–273.
[27] X. Mao, E. Seidlitz, K. Ghosh, et al., The cytoplasmic domain is critical to the tumor suppressor activity of TSLC1 in non-small cell lung cancer, Cancer Res. 63 (2003) 7979–7985.
[28] X. Mao, E. Seidlitz, R. Truant, et al., Re-expression of TSLC1 in a non-small-cell lung cancer cell line induces apoptosis and inhibits tumor growth, Oncogene 23 (2004) 5632–5642.
[29] M. Masuda, S. Kikuchi, T. Maruyama, et al., Tumor suppressor in lung cancer (TSLC)1 suppresses epithelial cell scattering and tubulogenesis, J. Biol. Chem. 280 (2005) 42164–42171.

Bioorganic & Medicinal Chemistry Letters 22 (2012) 4640–4644

Contents lists available at SciVerse ScienceDirect

Bioorganic & Medicinal Chemistry Letters

journal homepage: www.elsevier.com/locate/bmcl

Novel BACE1 inhibitors possessing a 5-nitroisophthalic scaffold at the P_2 position

Yoshio Hamada [a,b,*], Tomoya Nakanishi [b], Kenji Suzuki [b], Ryoji Yamaguchi [b], Takashi Hamada [b,d], Koushi Hidaka [a,b], Shoichi Ishiura [c], Yoshiaki Kiso [a,b,d,*]

[a] Faculty of Pharmaceutical Sciences, Kobe Gakuin University, Minatojima, Chuo-ku, Kobe 650-8586, Japan
[b] Center for Frontier Research in Medicinal Science, Kyoto Pharmaceutical University, Yamashina-ku, Kyoto 607-8412, Japan
[c] Department of Life Sciences, Graduate School of Arts and Sciences, University of Tokyo, Meguro-ku, Tokyo 153-8902, Japan
[d] Laboratory of Peptide Science, Nagahama Institute of Bio-Science and Technology, Tamura-cho, Nagahama 526-0829, Japan

ARTICLE INFO

Article history:
Received 25 April 2012
Revised 23 May 2012
Accepted 24 May 2012
Available online 1 June 2012

Keywords:
Alzheimer's disease
β-Secretase
BACE1
BACE1 inhibitor

ABSTRACT

Recently, we reported substrate-based pentapeptidic BACE1 inhibitors possessing a hydroxymethylcarbonyl isostere as a substrate transition-state mimic. These inhibitors showed potent inhibitory activities in enzymatic and cell assays. We also designed and synthesized non-peptidic and small-sized inhibitors possessing a heterocyclic scaffold at the P_2 position. By studying the structure–activity relationship of these inhibitors, we found that the σ–π interaction of an inhibitor with the BACE1-Arg235 side chain played a key role in the inhibition mechanism. Hence, we optimized the inhibitors with a focus on their P_2 regions. In this Letter, a series of novel BACE1 inhibitors possessing a 5-nitroisophthalic scaffold at the P_2 position are described along with the results of the related structure–activity relationship study. These small-sized inhibitors are expected improved membrane permeability and bioavailability.

Amyloid β (Aβ) peptide is a main component of senile plaques in the brains of Alzheimer's disease (AD) patients. According to the amyloid hypothesis,[1] β-secretase [BACE1: β-site APP (amyloid precursor protein) cleaving enzyme 1] appears promising as a molecular target for therapeutic intervention in AD,[2–6] as BACE1 triggers Aβ peptide formation by cleaving APP at the Aβ domain N-terminus.[7–12] Potent peptidic BACE1 inhibitors[13–19] (IC_{50} ~1.2 nM) with a hydroxymethylcarbonyl (HMC) isostere as a substrate transition-state mimic have been reported.[20,21] Of these inhibitors, KMI-429 exhibited effective inhibition of BACE1 activity in cultured cells and significant reduction of Aβ production in vivo (via direct administration into the hippocampi of APP transgenic and wild-type mice).[14b] Some natural amino acids in these inhibitors seem to be required to improve both enzymatic stability in vivo and permeability across the blood–brain barrier. Recently, with the goal of developing a practical anti-AD drug, non-peptidic and small-sized BACE1 inhibitors possessing a 2,6-pyridinedicarboxylic or chelidonic scaffold at the P_2 position were designed based on the conformer structure of a virtual inhibitor docked on the enzyme (Fig. 1), so called 'in silico conformational structure-based design'.[20] As these non-peptidic inhibitors exhibited lower inhibitory activities than peptidic KMI-compounds, more potent forms were desired and, thus, inhibitors possessing a halogen atom on the P_2-pyridine ring were designed by focusing on their interaction with the guanidino π-orbital of BACE1-Arg235 (Fig. 2), and found to be more potent.[23] In this study, we designed and synthesized novel BACE1 inhibitors possessing a 5-nitroisophthalic scaffold at their P_2 position by focusing on the interaction with side

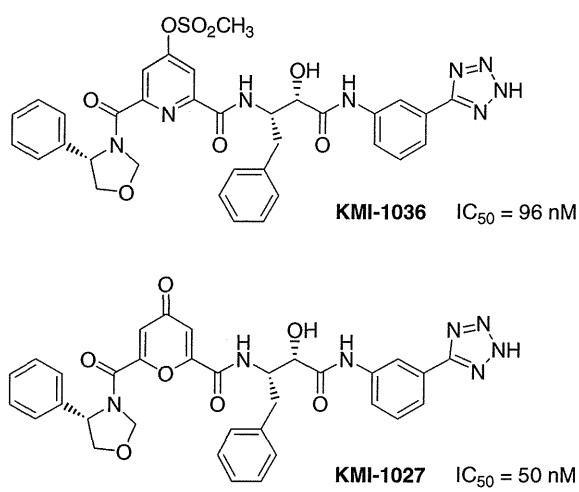

Figure 1. BACE1 inhibitors with a P_2 heterocyclic scaffold.

* Corresponding authors. Tel.: +81 749 64 8113; fax: +81 749 64 8140.
E-mail address: y_kiso@nagahama-i-bio.ac.jp (Y. Kiso).

0960-894X/$ - see front matter © 2012 Elsevier Ltd. All rights reserved.
http://dx.doi.org/10.1016/j.bmcl.2012.05.089

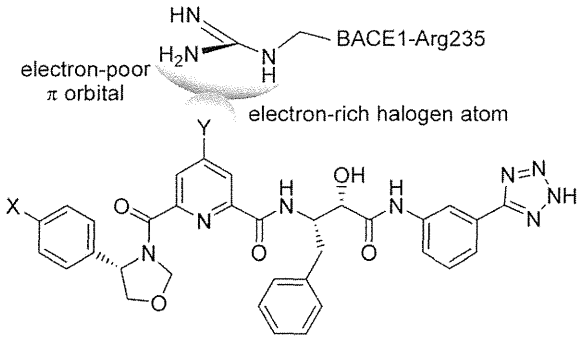

KMI-1237 (X = H, Y = Cl) IC_{50} = 22 nM
KMI-1256 (X = H, Y = Br) IC_{50} = 15 nM
KMI-1293 (X = H, Y = I) IC_{50} = 24 nM
KMI-1283 (X = F, Y = Cl) IC_{50} = 13 nM
KMI-1303 (X = F, Y = Br) IC_{50} = 9 nM
KMI-1302 (X = F, Y = I) IC_{50} = 10 nM

Figure 2. BACE1 inhibitors with a halogen atom on the P_2 aromatic ring.

chain of BACE1-Arg235. In addition, the results of their structure–activity relationship are discussed.

When the publicly-available X-ray crystal structures of BACE1-inhibitor complexes are compared, surprisingly, the guanidino-planes of Arg235-BACE1 show similar features in terms of flopping over the P_2 region of the inhibitors, and the nearest distances between the P_2 region and guanidino-plane show similar values of about 3 Å in the X-ray crystal structures of most BACE1-inhibitor complexes.[23] It was hypothesized here that the guanidino-plane of Arg235 pushes down on the P_2 region of the inhibitors, causing them to be affixed in the BACE1 active site, and that a slightly attractive force from a quantum effect, such as stacking or σ–π interactions, plays a significant role for packing down the inhibitors effectively in the active site of BACE1. Hence, an inhibitors, KMI-1303, was designed, which possessed a halogen atom on the P_2-pyridine scaffold, and proved to be quite potent (Fig. 2). The electron-rich halogen atom appeared able to interact with the electron-poor π-orbital of guanidino-plane by Coulomb's force. With the goal of identifying other forms of potent inhibitors by optimizing the inhibitor P_2 regions, we investigated the effect of other P_2 regions substituents which allowed to interact with the guanidino-plane of BACE1-Arg235. A 5-isophthalic scaffold was adopted as a P_2 residue for the synthesis of a series of BACE1 inhibitors.

BACE1 inhibitors **1–34** were synthesized with the plan to connect in tandem the blocks corresponding to the P_3–P_2 residues and P_1–P_1' residues (Scheme 1A) or to connect sequentially from the P_1' residues to P_3 residues (Scheme 1B). Amide bonds were produced by common solution-phase synthesis methods using 1-ethyl-3-(3-dimethylaminopropyl)carbodiimide·HCl (EDC·HCl) in the presence of 1-hydroxybenzotriazole (HOBt) as a coupling agent. For examples, in the synthesis of inhibitors **10** and **32** (Scheme 1), P_3 amine **37** and 5-nitroisophthalic acid were coupled to produce the P_3–P_2 residue **38**, with the former compound, possessing an oxazolidine ring, prepared from the corresponding amino alcohol, itself previously prepared from L-amino acid derivatives. Other amines were commercially available. P_1–P_1' residue **40** was synthesized from Boc-Apns-OH **39** [Apns: (2*S*,3*S*)-3-amino-2-hydroxy-4-phenylbutyric acid] and 5-(3-aminophenyl)tetrazole. Eventually, P_3–P_2 residue **38** and P_1–P_1' residue **40** were coupled to produce inhibitor **10**. Alternatively, some inhibitors, **32** for example, were synthesized from compound **40** by sequential connection with the P_2 residue and P_3 amine. BACE1 inhibitor **2** was synthesized from its methyl ester, by alkaline hydrolysis, which was prepared from monomethyl ester of benzene-1,3,5-tricarboxylic acid as a starting material. BACE1 inhibitor **4** was synthesized from compound **9** by catalytic hydrogenation using 5% Pd-C catalyst. All inhibitors were purified by preparative reversed phase-high performance liquid chromatography. BACE1 inhibitory activities of the synthesized inhibitors were determined

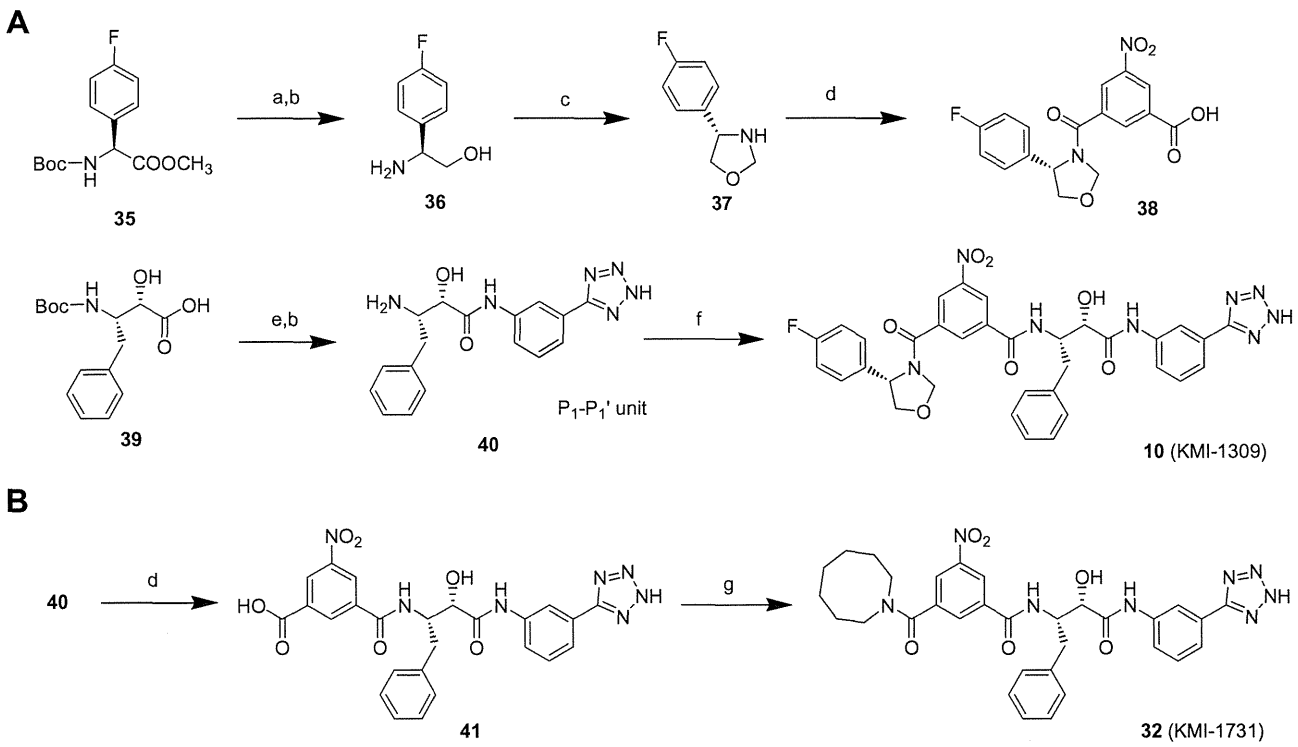

Scheme 1. Reagents and conditions: (a) $LiBH_4$/THF-MeOH; (b) 4 N HCl/dioxane; (c) HCHO, water; (d) 5-nitroisophthalic acid, EDC·HCl, HOBt/DMF; (e) 5-(3-aminophenyl)tetrazole, EDC·HCl, HOBt/DMF; (f) **38**, EDC·HCl, HOBt/DMF; (g) azocane, EDC·HCl, HOBt/DMF.

Table 1
BACE1 inhibitors possessing a chelidonic scaffold at the P_3 position

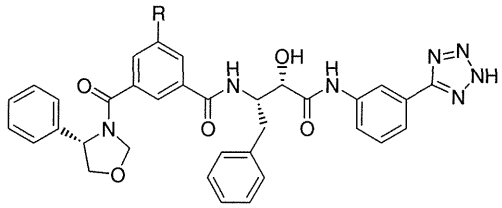

Compound (KMI-No.)	R	BACE1 inhibition %		IC_{50} (nM)
		at 2 μM	at 0.2 μM	
1 (KMI-1662)	-H	85	46	192
2 (KMI-1767)	-COOH	91	60	122
3 (KMI-1298)	$-OCOCH_3$	79	–	–
4 (KMI-1307)	$-NH_2$	49	–	–
5 (KMI-1280)	-Br	98	84	25
6 (KMI-1287)	-I	98	78	34
7 (KMI-1325)	$-CH_3$	95	65	67
8 (KMI-1277)	$-C(CH_3)_3$	63	–	–
9 (KMI-1214)	$-NO_2$	98	88	19

by an enzymatic assay using a recombinant human BACE1 and FRET (fluorescence resonance energy transfer) substrate as previously reported.[5,13–19,22,23]

First, BACE1 inhibitors **1–9** were synthesized possessing an isophthalic scaffold at the P_2 position and diverse groups on its aromatic ring (Table 1). Of these inhibitors, compound **9**, with a nitro group, exhibited the highest BACE1 inhibitory activity and compound **5**, **6**, and **7**, possessing a halogen atom or methyl group on the P_2 aromatic ring, also exhibited high BACE1 inhibitory activities, suggesting that a small-sized and hydrophobic substituent on the P_2 aromatic ring was preferential for BACE1 inhibition. Having previously reported the nature of a series of BACE1 inhibitors possessing a halogen atom on the P_2-heterocyclic scaffold, the focus here was on the nitro-group as a P_2-substituent, resulting in the design of inhibitors **10–34**. Inhibitors **10–24** possessed a 5-membered oxazolidine ring (Table 2) and, of these, compound **10** exhibited the highest BACE1 inhibitory activity, followed in activity by compounds **17–19** and **22**. The results also showed that compound **16**, with a small-sized group and compounds **13**, **15**, and **24**, with bulky oxazolidine ring substituents, showed low inhibitory activities, suggesting that size—being the length of as phenyl group—and planarity for an inhibitor P_2-substituent are important. In particular, a *p*-fluorophenyl group appeared to interact tightly with the BACE1 S_3 sub-pocket.

Next, inhibitors **25–34**, with no oxazolidine ring at the P_3 position were synthesized (Table 3). Inhibiters **26** and **27**, with a P_2-benzylamino type group, exhibited relatively high BACE1 inhibitory activities and, although compound **28** with a P_3-pyrrolidine ring, showed low inhibitory activity, inhibitor **29**, possessing a substituent on the P_3-pyrrolidine ring, showed superior inhibitory activity. This suggested that there was an empty space between the P_3-pyrrolidine ring and S_3 pocket of BACE1. Hence, inhibitors **30–34** were produced with cyclic amines at the P_3 position and, of these, compound **32** (KMI-1731), with an 8-memberd ring, showed the highest inhibitory activity. To understand these results, a docking simulation study was performed using MOE soft-

Table 2
BACE1 inhibitors possessing a 2,6-pyridinedicarboxylic scaffold at the P_3 position

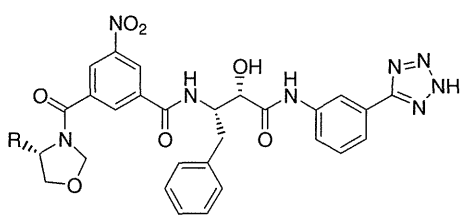

Compound (KMI-No.)	R	BACE1 inhibition %		IC_{50} (nM)
		at 2 μM	at 0.2 μM	
10 (KMI-1309)	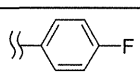	99	91	13
11	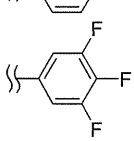	81	41	–
12	Benzyl	89	45	–
13	Cyclohexylmethyl	50	–	–
14	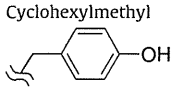	80	–	–
15	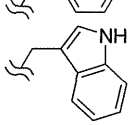	57	–	–
16	$-CH_3$	33	–	
17	-Et	92	54	
18	-*n*-Pr	93	57	
19	-*n*-Bu	92	59	
20	Isopropyl	88	44	
21	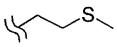	86	45	
22	*sec*-Butyl	94	62	
23	Isobutyl	85	42	
24	*tert*-Butyl	71	–	

Table 3
BACE1 inhibitors possessing 2,6-pyridinedicarboxylic scaffold at the P_3 position

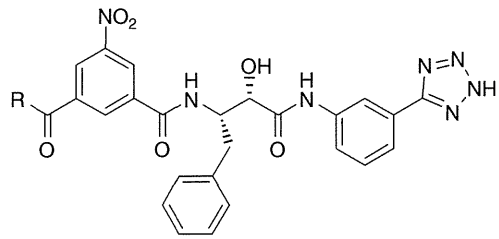

Compound (KMI-No.)	R	BACE1 inhibition %		Compound (KMI-No.)	R	BACE1 inhibition %	
		at 2 μM	at 0.2 μM			at 2 μM	at 0.2 μM
25-(KMI-1211)	-N(*n*-Pr)$_2$	79	–	**30** (KMI-1729)	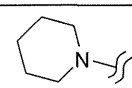	49	–
26 (KMI-1212)	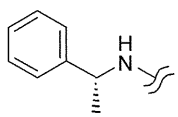	83	44	**31**-(KMI-1730)	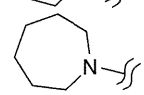	60	–
27 (KMI-1213)	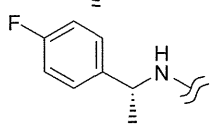	87	50	**32** (KMI-1731)	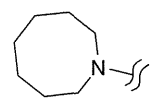	80	38
28 (KMI-1728)	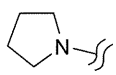	24	–	**33** (KMI-1769)	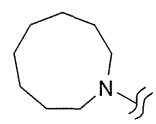	28	–
29 (KMI-1219)	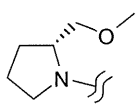	89	57	**34** (KMI-1732)	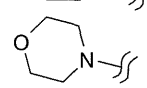	0	–

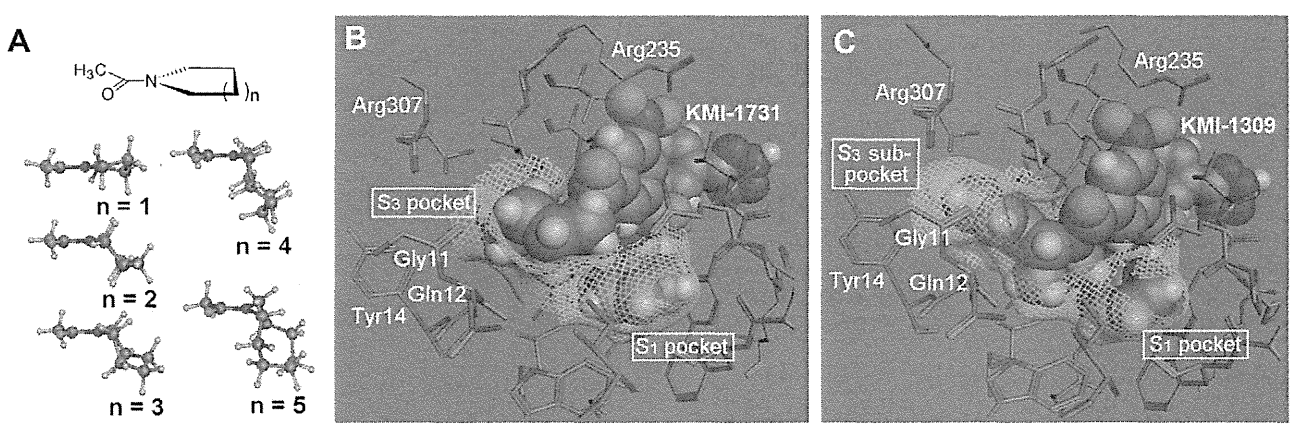

Figure 3. (A) Configurations of some cyclic amides. (B) Inhibitor **32** (KMI-1731) docked in BACE1. (C) Inhibitor **10** (KMI-1309) docked in BACE1 (PDB ID: 2B8L). Space-filing models and green lines indicate inhibitors and BACE1 hydrophobic pockets, respectively, and stick models indicate BACE1 amino acid residues around each inhibitor.

ware (Chemical Computing Group Inc., Canada, Figure 3). The configurations of cyclic acetyl amides from 5- to 9-membered rings after energy minimization under the MMFF94x force field are shown in Figure 3A. The molecular sizes of these cyclic acetyl amides appeared to be similar in the direction of the amide bonds regardless of their ring-sizes, because the larger rings present more greatly curved configurations. When inhibitor **32**, with an 8-membered ring, was docked in BACE1, this ring appeared to interact tightly with the S_3 pocket of BACE1 due to its very bent structure (Fig. 3B). However, compound **33**, with a 9-membered ring, showed surprisingly low inhibitory activity. In general, an odd-membered, medium-sized ring has higher strain energy and no symmetric properties, resulting in a bulky configuration (Figure 3A). Consequently, compound **33** might not have been able to bind to the S_3 pocket of BACE1. On the other hand, compound **34,** with a P_3-morpholine ring, exhibited no inhibitory activity, suggesting that a hydrophilic moiety, such as an oxygen atom, could not interact with the hydrophobic S_3 pocket of BACE1. For comparison, BACE1 docked inhibitor **10** is shown in Figure 3C. Inhibitor **32**'s P_3 moiety could have interacted with the S_3 pocket of BACE1, while inhibitor **10**'s P_3-benzene ring appeared able to interact effectively with the S_3 sub-pocket lying behind the S_3 pocket.

As described above, inhibitors with a nitro group on the P_2-isophthalic scaffold exhibited the highest inhibitory activities among the present inhibitors possessing an isophthalic scaffold. To better understand this finding, a docking simulation performed using MOE software. As inhibitor **5–7** exhibited potent BACE1 inhibitory activities, a halogen and methyl groups were speculated

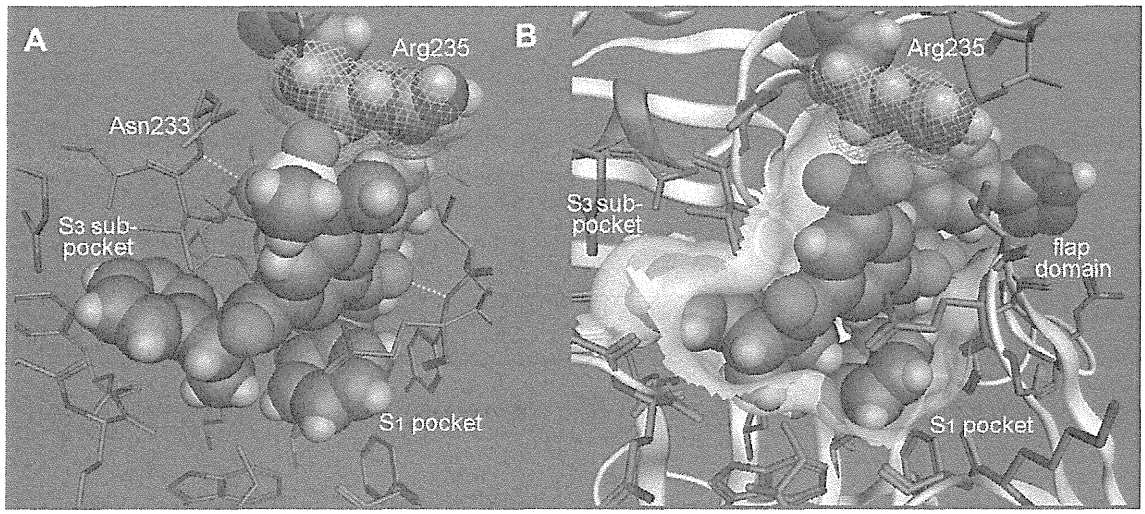

Figure 4. Interaction between BACE1-Arg235 and inhibitors docked in BACE1 (PDB ID: 2B8L). (A) Merck's compound. (B) Compound **10** (KMI-1309). Inhibitors and Arg235 were depicted by space-filling models. Stick models indicate BACE1 amino acid residues around each inhibitor.

to be fixed on the P_2-isophthalic ring by direct covalent bonding and effectively bound to the guanidino-plane of BACE1-Arg235 by σ–π interactions. The X-ray crystal structure of Merck's inhibitor bound in BACE1 (PDB ID: 2B8L) is shown in Figure 4A. Because the sulfonyl-oxygen atom of P_2-*N*-methyl-*N*-methanesulfonyl group of Merck's inhibitor appears to interact with the α-amino group of BACE1-Asn233 by hydrogen bonding, the *N*-methyl group is fixed on the P_2-isophthalic ring and might bind effectively to the BACE1-Arg235 by CH–π interactions. Considering the nitro group on the P_2-isophthalic ring of inhibitor **10** (Fig. 4B), the rotation of a nitro group on an aromatic ring is restricted by resonance effects and is thus fixed on its ring. For this reason, the oxygen atom of the nitro group is speculated here to be fixed on the P_2-isophthalic ring and can thus effectively bind to BACE1-Arg235 by O–π interactions.

In conclusion, we synthesized a series of BACE1 inhibitors possessing an isophthalic scaffold at the P_2 position, and found some potent BACE1 inhibitors with a nitro group on the P_2 ring. Notably, inhibitor **10** (KMI-1309) was shown to have potent BACE1 inhibitory activity (IC_{50} = 13 nM). These small-sized and non-peptidic inhibitors are expected to provide improvement of clinical inhibitor bioavailability and membrane permeability across the blood–brain barrier.

Acknowledgments

This study was supported in part by the Grants-in-Aid for Scientific Research (A) and (C) from MEXT (Ministry of Education, Culture, Sports, Science and Technology), Japan. (KAKENHI No.21249007 and No.23590137, respectively) We thank T. Hamada and Dr. J.-T. Nguyen for performing the in vitro enzyme assays and his help in preparing the manuscript, respectively.

References and notes

1. (a) Hong, L.; Koelsch, G.; Lin, X.; Wu, S.; Terzyan, S.; Ghosh, A. K.; Zhang, X. C.; Tang, J. *Science* **2000**, *290*, 150; (b) Sipe, J. D. *Annu. Rev. Biochem.* **1992**, *61*, 947; (c) Selkoe, D. J. *Ann. N.Y. Acad. Sci.* **2000**, *924*, 17; (d) Steiner, H.; Capell, A.; Leimer, U.; Haass, C. *Eur. Arch. Psychiatric Clin. Neurosci.* **1999**, *249*, 266; (e) Selkoe, D. J. *Ann. Med.* **1989**, *21*, 73.
2. (a) Ghosh, A. K.; Shin, D.; Downs, D.; Koelsch, G.; Lin, X.; Ermolieff, J.; Tang, J. *J. Am. Chem. Soc.* **2000**, *122*, 3522; (b) Ghosh, A. K.; Bilcer, G.; Harwood, C.; Kawahara, R.; Shin, D.; Hussain, K. A.; Hong, L.; Loy, J. A.; Nguyen, C.; Koelsch, G.; Ermolieff, J.; Tang, J. *J. Med. Chem.* **2001**, *44*, 2865.
3. Tung, J. S.; Davis, D. L.; Anderson, J. P.; Walker, D. E.; Mamo, S.; Jewett, N.; Hom, R. K.; Sinha, S.; Thorsett, E. D.; John, V. *J. Med. Chem.* **2002**, *45*, 259.
4. Tamamura, H.; Kato, T.; Otaka, A.; Fujii, N. *Org. Biomol. Chem.* **2003**, *1*, 2468.
5. Shuto, D.; Kasai, S.; Kimura, T.; Liu, P.; Hidaka, K.; Hamada, T.; Shibakawa, S.; Hayashi, Y.; Hattori, C.; Szabo, B.; Ishiura, S.; Kiso, Y. *Bioorg. Med. Chem. Lett.* **2003**, *13*, 4273.
6. (a) Hamada, Y.; Kiso, Y. *Expert Opin. Drug Discov.* **2009**, *4*, 391; (b) Ziora, Z.; Kimura, T.; Kiso, Y. *Drugs Future* **2006**, *31*, 53; (c) Nguyen, J.-T.; Yamani, A.; Kiso, Y. *Curr. Pharm. Design* **2006**, *12*, 4309.
7. Vassar, R.; Bennett, B. D.; Babu-Khan, S.; Kahn, S.; Mendiaz, E. A.; Denis, P.; Teplow, D. B.; Ross, S.; Amarante, P.; Loeloff, R.; Luo, Y.; Fisher, S.; Fuller, J.; Edenson, S.; Lile, J.; Jarosinski, M. A.; Biere, A. L.; Curran, E.; Burgess, T.; Louis, J. C.; Collins, F.; Treanor, J.; Rogers, G.; Citron, M. *Science* **1999**, *286*, 735.
8. Yan, R.; Bienkowski, M. J.; Shuck, M. E.; Miao, H.; Tory, M. C.; Pauley, A. M.; Brashier, J. R.; Stratman, N. C.; Mathews, W. R.; Buhl, A. E.; Carter, D. B.; Tomasselli, A. G.; Parodi, L. A.; Heinrikson, R. L.; Gurney, M. E. *Nature* **1999**, *402*, 533.
9. Sinha, S.; Anderson, J. P.; Barbour, R.; Basi, G. S.; Caccavello, R.; Davis, D.; Doan, M.; Dovey, H. F.; Frigon, N.; Hong, J.; Jacobson-Croak, K.; Jewett, N.; Keim, P.; Knops, J.; Lieberburg, I.; Power, M.; Tan, H.; Tatsuno, G.; Tung, J.; Schenk, D.; Seubert, P.; Suomensaari, S. M.; Wang, S.; Walker, D.; Zhao, J.; McConlogue, L.; John, V. *Nature* **1999**, *402*, 537.
10. Hussain, I.; Powell, D.; Howlett, D. R.; Tew, D. G.; Meek, T. D.; Chapman, C.; Gloger, I. S.; Murphy, K. E.; Southan, C. D.; Ryan, D. M.; Smith, T. S.; Simmons, D. L.; Walsh, F. S.; Dingwall, C.; Christie, G. *Mol. Cell. Neurosci.* **1999**, *14*, 419.
11. Selkoe, D. J. *Nature* **1999**, *399*, A23.
12. Sinha, S.; Lieberburg, I. *Proc. Natl. Acad. Sci. U.S.A.* **1999**, *96*, 11049.
13. Kimura, T.; Shuto, D.; Kasai, S.; Liu, P.; Hidaka, K.; Hamada, T.; Hayashi, Y.; Hattori, C.; Asai, M.; Kitazume, S.; Saido, T. C.; Ishiura, S.; Kiso, Y. *Bioorg. Med. Chem. Lett.* **2004**, *14*, 1527.
14. (a) Kimura, T.; Shuto, D.; Hamada, Y.; Igawa, N.; Kasai, S.; Liu, P.; Hidaka, K.; Hamada, T.; Hayashi, Y.; Kiso, Y. *Bioorg. Med. Chem. Lett.* **2005**, *15*, 211; (b) Asai, M.; Hattori, C.; Iwata, N.; Saido, T. C.; Sasagawa, N.; Szabó, B.; Hashimoto, Y.; Maruyama, K.; Tanuma, S.; Kiso, Y.; Ishiura, S. *J. Neurochem.* **2006**, *96*, 533.
15. Kimura, T.; Hamada, Y.; Stochaj, M.; Ikari, H.; Nagamine, A.; Abdel-Rahman, H.; Igawa, N.; Hidaka, K.; Nguyen, J-T.; Saito, K.; Hayashi, Y.; Kiso, Y. *Bioorg. Med. Chem. Lett.* **2006**, *16*, 2380.
16. Hamada, Y.; Igawa, N.; Ikari, H.; Ziora, Z.; Nguyen, J.-T.; Yamani, A.; Hidaka, K.; Kimura, T.; Saito, K.; Hayashi, Y.; Ebina, M.; Ishiura, S.; Kiso, Y. *Bioorg. Med. Chem. Lett.* **2006**, *16*, 4354.
17. Hamada, Y.; Abdel-Rahman, H.; Yamani, A.; Nguyen, J.-T.; Stochaj, M.; Hidaka, K.; Kimura, T.; Hayashi, Y.; Saito, K.; Ishiura, S.; Kiso, Y. *Bioorg. Med. Chem. Lett.* **2008**, *18*, 1649.
18. Hamada, Y.; Tagad, H. D.; Nishimura, Y.; Ishiura, S.; Kiso, Y. *Bioorg. Med. Chem. Lett.* **2012**, *22*, 1130.
19. Hamada, Y.; Ishiura, S.; Kiso, Y. *Bioorg. ACS Med. Chem. Lett.* **2012**, *3*, 193.
20. Mimoto, T.; Imai, J.; Tanaka, S.; Hattori, N.; Takahashi, O.; Kisanuki, S.; Nagano, Y.; Shintani, M.; Hayashi, H.; Akaji, K.; Kiso, Y. *Chem. Pharm. Bull.* **1991**, *39*, 2465.
21. Mimoto, T.; Imai, J.; Tanaka, S.; Hattori, N.; Kisanuki, S.; Akaji, K.; Kiso, Y. *Chem. Pharm. Bull.* **1991**, *39*, 3088.
22. Hamada, Y.; Ohta, H.; Miyamoto, N.; Yamaguchi, R.; Yamani, A.; Hidaka, K.; Kimura, T.; Saito, K.; Hayashi, Y.; Ishiura, S.; Kiso, Y. *Bioorg. Med. Chem. Lett.* **2008**, *18*, 1654.
23. Hamada, Y.; Ohta, H.; Miyamoto, N.; Sarma, D.; Hamada, T.; Nakanishi, T.; Yamasaki, M.; Yamani, A.; Hidaka, K.; Ishiura, S.; Kiso, Y. *Bioorg. Med. Chem. Lett.* **2009**, *19*, 2435.

Bioorganic & Medicinal Chemistry Letters 22 (2012) 1130–1135

Contents lists available at SciVerse ScienceDirect

Bioorganic & Medicinal Chemistry Letters

journal homepage: www.elsevier.com/locate/bmcl

Tripeptidic BACE1 inhibitors devised by in-silico conformational structure-based design

Yoshio Hamada [a,b,*], Harichandra D. Tagad [b], Yoshinori Nishimura [b], Shoichi Ishiura [c], Yoshiaki Kiso [a,b,d,*]

[a] Faculty of Pharmaceutical Sciences, Kobe Gakuin University, Minatojima, Chuo-ku, Kobe 650-8586, Japan
[b] Center for Frontier Research in Medicinal Science, Kyoto Pharmaceutical University, Yamashina-ku, Kyoto 607-8412, Japan
[c] Department of Life Sciences, Graduate School of Arts and Sciences, University of Tokyo, Meguro-ku, Tokyo 153-8902, Japan
[d] Department of Bio-Science, Nagahama Institute of Bio-Science and Technology, Tamura-cho, Nagahama 526-0829, Japan

ARTICLE INFO

Article history:
Received 7 October 2011
Accepted 25 November 2011
Available online 1 December 2011

Keywords:
Alzheimer's disease
β-Secretase
BACE1
BACE1 inhibitor

ABSTRACT

Previously reported pentapeptidic BACE1 inhibitors, designed using a substrate-based approach, were used as lead compounds for the further design of non-peptidic BACE1 inhibitors. Although these peptidic and non-peptidic inhibitors, with a hydroxymethylcarbonyl isostere as a substrate transition-state mimic, exhibited potent BACE1 inhibitory activities, their molecular-sizes appeared a little too big (molecular weight of >600 daltons) for developing practical anti-Alzheimer's disease drugs. To develop lower weight BACE1 inhibitors, a series of tripeptidic BACE1 inhibitors were devised using a design approach based on the conformation of a virtual inhibitor bound to the BACE1 active site, also called 'in-silico conformational structure-based design'. Although these tripeptidic BACE1 inhibitors contained some natural amino acid residues, they are expected to be useful as lead compounds for developing the next generation BACE1 inhibitors, due to their low molecular size and unique structural features compared with previously reported inhibitors.

Amyloid β peptide (Aβ), the main component of senile plaques in the brains of Alzheimer's disease (AD) patients,[1] is formed by proteolysis of amyloid precursor protein (APP).[2,3] As β-site APP cleaving enzyme 1 (BACE1, also known as β-secretase) triggers Aβ formation by cleavage at the Aβ domain *N*-terminus,[4–7] it is a molecular target for AD therapeutic intervention.[8–11] In recent reports on pentapeptidic and non-peptidic BACE1 inhibitors,[11–16] peptidic inhibitors KMI-420, -429, -684, and -574 (Fig. 1), which contained phenylnorstatine (Pns: (2*R*,3*S*)-3-amino-2-hydroxy-4-phenylbutyric acid) as a substrate transition-state mimic, showed potent BACE1 inhibitory activities.[17,18] Of these, KMI-429 exhibited effective activity in cultured cells and a significant reduction of Aβ production in vivo (by direct administration into APP transgenic and wild-type mice hippocampi).[13] However, some natural amino acid residues in these inhibitors appear necessary for the enzymatic stability in vivo and blood–brain barrier permeability needed to be practical drugs. Accordingly here, non-peptidic BACE1 inhibitors were designed which possessed a heterocyclic scaffold, such as a chelidamic or 2,5-pyridinedicarboxylic moiety, at the P_2 position using 'in-silico conformational structure-based design'.[19] Furthermore, through focusing on interaction with the BACE1-Arg235 side chain, the non-peptidic inhibitor KMI-1303, possessing a halogen atom on the P_2-pyridine scaffold, was designed and found to be a potent inhibitor (Fig. 2). Although these pentapeptidic and non-peptidic BACE1 inhibitors showed potent inhibitory activities, their molecular weights were considered a little high (>600 daltons) for practical anti-AD drugs. With the goal of developing low molecular weight and thus smaller inhibitors, the location of two catalytic Asp residues in BACE1 were examined. As all of the BACE1 active site pockets are created by closure of the flap domain (Fig. 3A), effective, potential inhibitors might involve fixing the 'closed-form' of the flap domain. Additionally, the two catalytic Asp residues are located at some distance from the flap domain (Fig. 3B). Thus, the interactions of the P'_1 region and substrate transition-state analogue with the corresponding pockets of BACE1 were hypothesized to be unnecessary for fixing the flap domain. As most existing BACE1 inhibitors have been designed to optimize interactions with the flap domain and the two catalytic Asp residues, they have naturally had high molecular weights to span the separation. The possible design of an inhibitor lacking the P'_1 position and substrate transition-state analogue was speculated here such that it could stabilize the folding pose around the inhibitor's P_1 phenyl group (Fig. 4B). Previously reported from here, a design tool focused on the conformation of a virtual inhibitor bound in the BACE1 active site was used to allow the synthesis of non-peptidic BACE1 inhibitors.[19] The well known concept that the stability of a specific conformer of a medicine is crucially important for proper drug effect has been employed in computational studies for drug design. In fact, common molecular dynamics calculations

* Corresponding authors. Tel.: +81 749 64 8113; fax: +81 749 64 8140.
E-mail address: y_kiso@nagahama-i-bio.ac.jp (Y. Kiso).

0960-894X/$ - see front matter © 2011 Elsevier Ltd. All rights reserved.
doi:10.1016/j.bmcl.2011.11.102

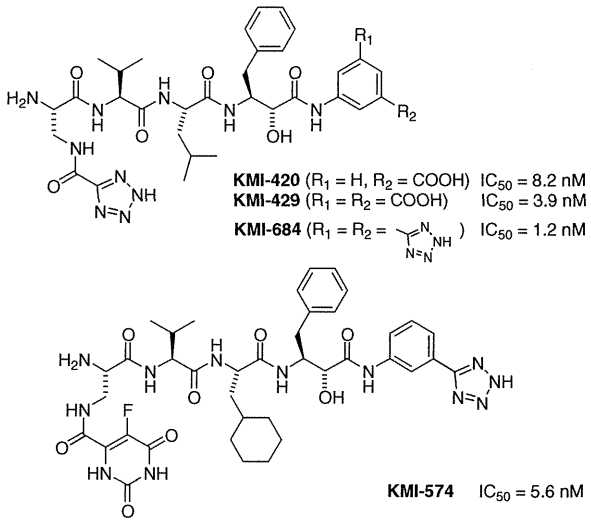

Figure 1. Pentapeptidic BACE1 inhibitor structures.

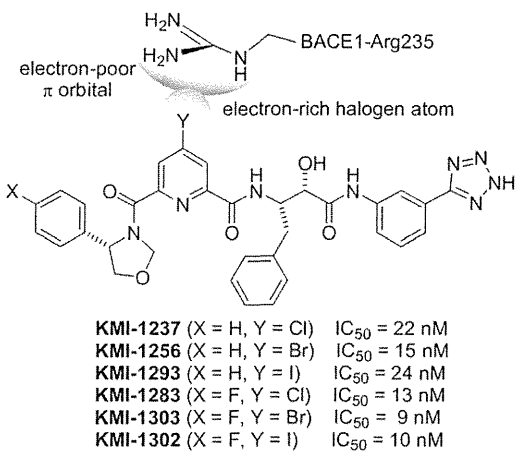

Figure 2. BACE1 inhibitor structures with a halogen atom on the P_2 aromatic ring.

or docking simulation software produce the potential energy values of drug molecules using descriptors regarding steric energy. On the other hand, the design tool used here, 'in-silico conformational structure-based design', is employed as a problem-solving tool for identifying drug candidates. In this study, the proposition of how to design low molecular weight inhibitors lacking a P'_1 moiety and substrate transition-state analogue was solved by seeking to stabilize the folding structure around the P_1-phenyl ring of a virtual inhibitor. For steric energy calculations, low molecular weight model compounds were used to exclude the effect of their intramolecular interactions in solution (Fig. 4A), because an inhibitor docked in the enzyme's active site generally interacts with the pocket of enzyme, not within the inhibitor molecule. Dihedral energy plots were constructed by rotating two covalent bonds, between the *C*-terminus amide bond and its side-by-side carbon atoms, of virtual compounds under an MMFF94x force field, using MOE software (Chemical Computing Group Inc., Canada). The optimal modification around the P_1 region of virtual inhibitors was then screened using a folding conformer by calculating their steric energy. A virtual inhibitor with two methyl groups at the P_1 position was found that showed a folding structure around the P_1-phenyl ring and a most-stable conformer which overlapped the red star symbol in the dihedral energy plot chart corresponding to an inhibitor docked on the enzyme (Fig. 4A); the folding structure appeared likely to be stabilized by a *gem*-dimethyl effect. A series of inhibitors were then designed which had a folding configuration around the P_1-phenyl ring.

BACE1 inhibitors **1–38** and **53–57** were synthesized by traditional solution-phase peptide synthesis methods, similar to previously reported procedures, from amines corresponding to the P_1 residue as starting materials and N-protected amino acids. Peptide bonds were formed sequentially using 1-ethyl-3-(3-dimethylaminopropyl)carbodiimide·HCl (EDC·HCl) in the presence of 1-hydroxybenzotriazole (HOBt) as a coupling agent.[11–16] For example, the synthesis of inhibitor **6** began with 2-methyl-1-phenylpropane-2-amine as the P_1-amine followed by peptide bond formation with selected amino acids and then protecting group removal (Scheme 1). Other P_1-amines were prepared from 2-methyl-1-phenylpropane-2-amine **39** or phenylacetic acids **44a–e** (Scheme 2). In particular, amines **41–43** were prepared from amine hydrochloride **40** by bromination, nitration and iodination, respectively, and amine **52** was prepared from amine **39** by catalytic hydrogenation using Adams' catalyst. Inhibitors **11–17**, **20**, **23–32**, **35**, and **36** were synthesized from P_2 – P_1 blocks **50a–b** or **51a–e** in a similar manner to above. P_2–P_1 blocks **50a–b** or **51a–e** were synthesized from alcohols **46a–e**, previously prepared from phenylacetic acids **44a–e** and nitriles **49a–b**. The latter two groups of reactants were prepared from corresponding Fmoc-protected amino-acid amides **48a–b**, using the Ritter reaction and the ensuing Fmoc-deprotec-

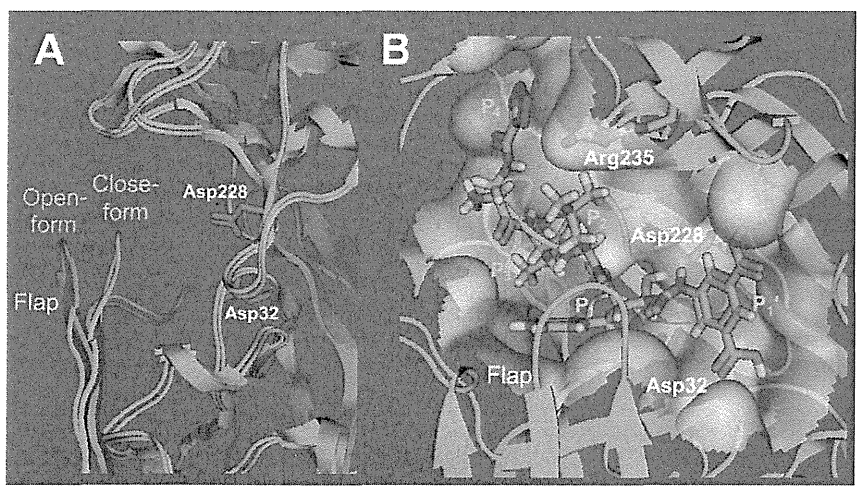

Figure 3. (A) Superimposed flap domain of 'open-form' (PDB ID: 1W50) and 'close-form' (PDB ID: 2B8L) of BACE1. (B) KMI-429 docked in BACE1 enzyme (PDB ID: 2B8L).

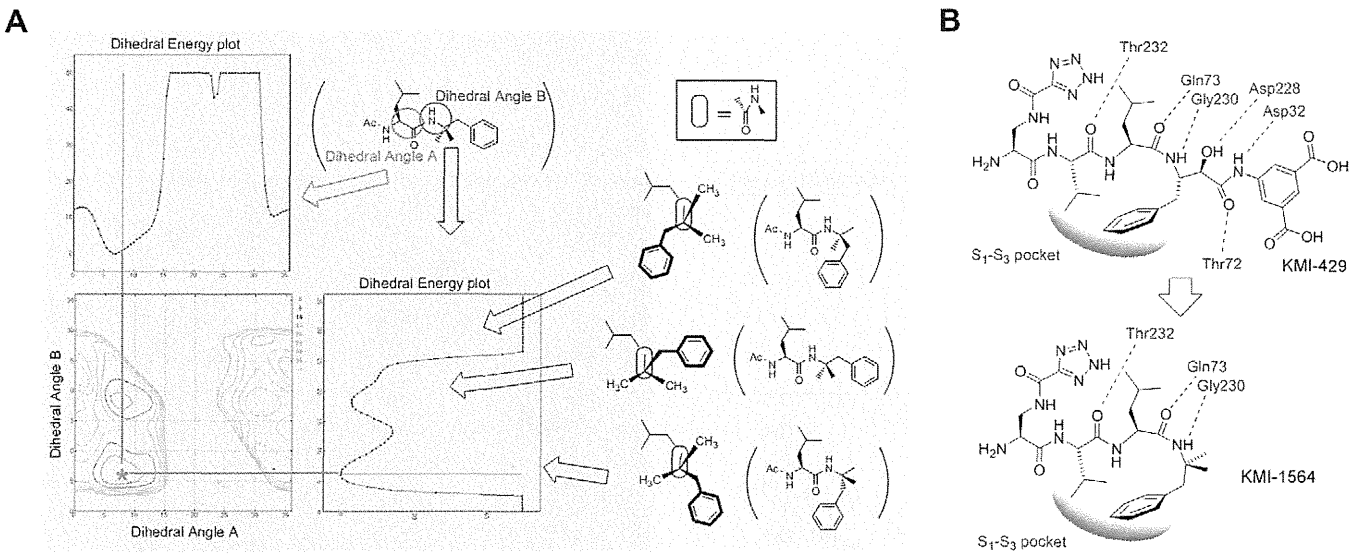

Figure 4. Design of tripeptidic BACE1 inhibitors. (A) Optimization of virtual inhibitor using in-silico conformational structure-based design, red star indicates configuration of inhibitor docked in BACE1. (B) Design of tripeptidic BACE1 inhibitor **3** (KMI-1564) from KMI-429 as parent compound.

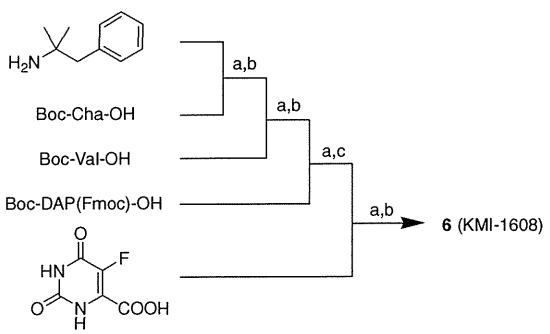

Scheme 1. Reagents and conditions: (a) EDC·HCl, HOBt/DMF; (b) 4 N HCl/dioxane; (c) 20% diethylamine/dioxane.

tion. All inhibitors were purified by preparative reversed phase-high performance liquid chromatography and their BACE1 inhibitory activity determined by an enzymatic assay using a recombinant human BACE1 and fluorescence resonance energy transfer substrate as previously reported.[11–16,19,20]

Inhibitor **3** (KMI-1564), containing the same P_2–P_4 residues as KMI-429, showed lower BACE1 inhibitory activity (70% inhibition at 2 μM) than KMI-429 (100% inhibition at 2 μM, IC_{50} = 3.9 nM) as shown in Table 1. With the reduction of interacting sites between inhibitor and BACE1 allowed by reducing the molecular weight (~70% compared with KMI-429), it appeared that inhibitor **3** and KMI-429 should have had similar affinity for the active site per unit molecular weight. Furthermore, the tripeptidic BACE1 inhibitor **6** (KMI-1608), designed for optimization at the P_4 and P_2 position, was found to be potent.

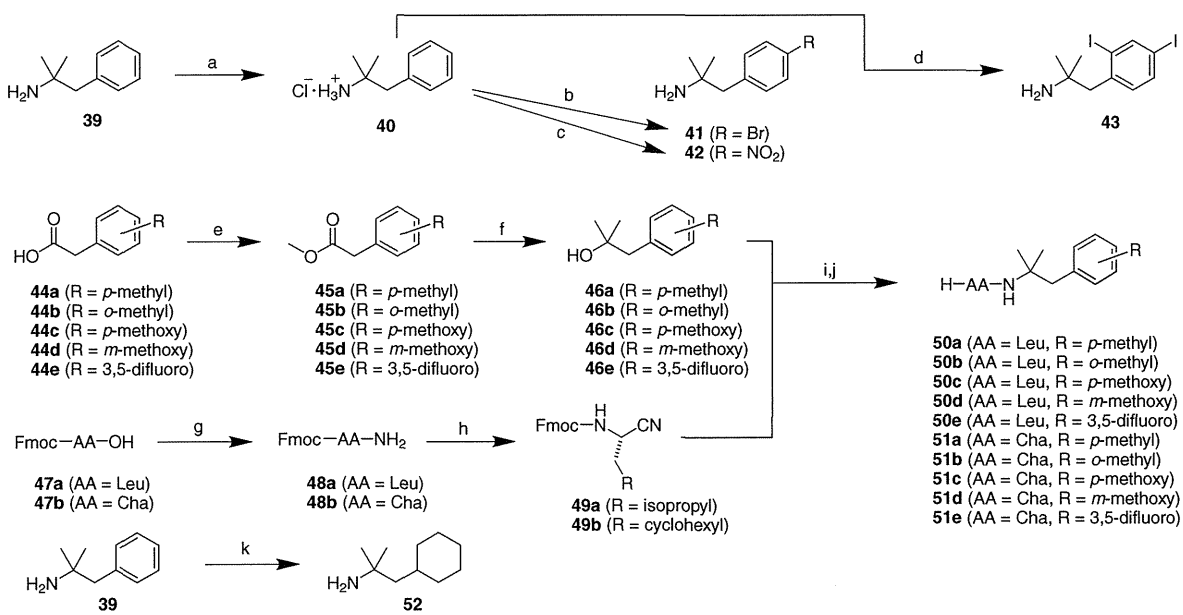

Scheme 2. Reagents and conditions: (a) 4 N HCl/dioxane; (b) Br_2, H_2O; (c) HNO_3, H_2SO_4; (d) I_2, $NaIO_4$, H_2SO_4; (e) $SOCl_2$, MeOH; (f) CH_3MgI, Et_2O; (g) NH_4HCO_3, EDC·HCl, DMF; (h) $(TFA)_2O$, pyridine, THF; (i) conc. H_2SO_4, CH_3COOH; (j) 20% Et_2NH/DMF; (k) H_2, PtO_2, AcOH.

Table 1
Tripeptidic BACE1 inhibitors

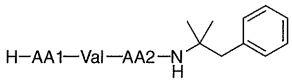

Compound (KMI-No.)	AA1[a]	AA2[b]	BACE1 inhibition % at 2 μM
1 (KMI-1563)	Glu	Leu	<10
2 (KMI-1606)	Glu	Cha	16
3 (KMI-1564)	A	Leu	70
4 (KMI-1607)	A	Cha	76
5 (KMI-1565)	B	Leu	90
6 (KMI-1608)	B	Cha	92
7 (KMI-1556)	C	Leu	77
8 (KMI-1609)	C	Cha	80

[a] Amino acids:

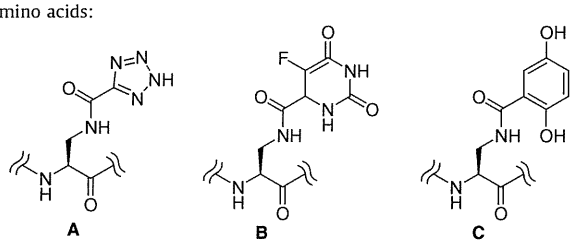

[b] Cha: L-cyclohexylalanine.

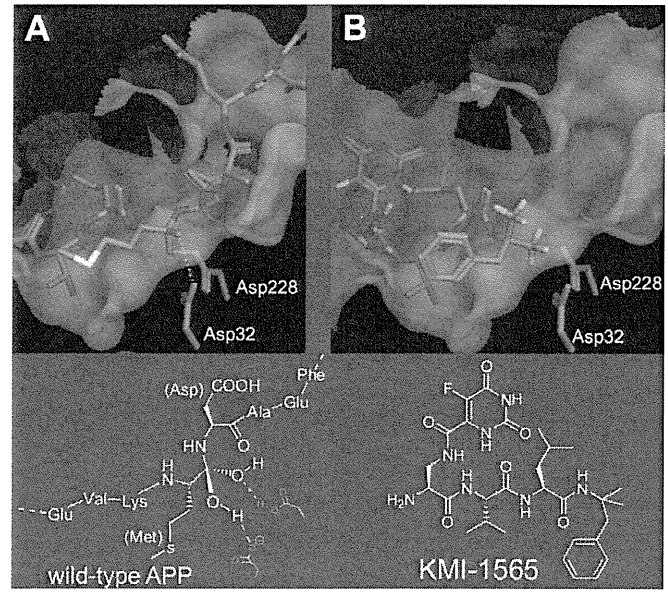

Figure 5. Docking simulation illustrations. (A) Substrate transition-state of APP (wild-type) docked in BACE1. (B) Inhibitor **5** (KMI-1565) docked in BACE1.

Table 2
Tripeptidic BACE1 inhibitors possessing substituents on the P_1-phenyl ring

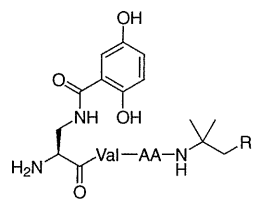

Compound (KMI-No.)	AA	R	BACE1 inhibition % at 2 μM
9 (KMI-1694)	Leu	*p*-Nitrophenyl	45
10 (KMI-1718)	Cha	*p*-Nitrophenyl	80
11 (KMI-1724)	Cha	*p*-Bromophenyl	81
12 (KMI-1887)	Leu	*p*-Methylphenyl	51
13 (KMI-1879)	Cha	*o*-Methylphenyl	54
14 (KMI-1866)	Leu	*p*-Methoxyphenyl	41
15 (KMI-1881)	Cha	*p*-Methoxyphenyl	45
16 (KMI-1883)	Leu	*m*-Methoxyphenyl	46
17 (KMI-1885)	Cha	*m*-Methoxyphenyl	49
18 (KMI-1726)	Leu	2,4-Diiodophenyl	78
19 (KMI-1778)	Cha	2,4-Diiodophenyl	88
20 (KMI-1897)	Leu	3,5-Difluorophenyl	59

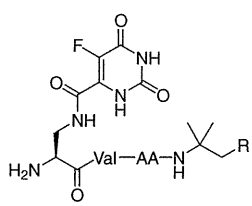

21 (KMI-1693)	Leu	*p*-Nitrophenyl	27
22 (KMI-1717)	Cha	*p*-Nitrophenyl	89
23 (KMI-1719)	Leu	*p*-Bromophenyl	85
24 (KMI-1723)	Cha	*p*-Bromophenyl	92
25 (KMI-1886)	Leu	*p*-Methylphenyl	86
26 (KMI-1895)	Cha	*p*-Methylphenyl	88
27 (KMI-1840)	Leu	*o*-Methylphenyl	91
28 (KMI-1878)	Cha	*o*-Methylphenyl	84
29 (KMI-1865)	Leu	*p*-Methoxyphenyl	83
30 (KMI-1880)	Cha	*p*-Methoxyphenyl	85
31 (KMI-1882)	Leu	*m*-Methoxyphenyl	84
32 (KMI-1884)	Cha	*m*-Methoxyphenyl	77

(*continued on next page*)

Table 2 (*continued*)

Compound (KMI-No.)	AA	R	BACE1 inhibition % at 2 μM
33 (KMI-1725)	Leu	2,4-Diiodophenyl	91
34 (KMI-1777)	Cha	2,4-Diiodophenyl	96
35 (KMI-1896)	Leu	3,5-Difluorophenyl	86
36 (KMI-1898)	Cha	3,5-Difluorophenyl	91
37 (KMI-1842)	Leu	Cyclohexyl	91
38 (KMI-1843)	Cha	Cyclohexyl	88

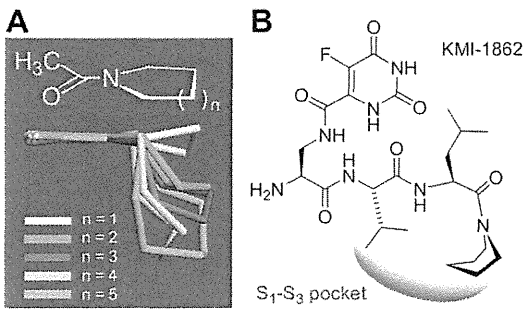

Figure 6. (A) Configuration of cyclic amides. (B) Design of tripeptidic BACE1 inhibitor possessing a cyclic amine at the *C*-terminus.

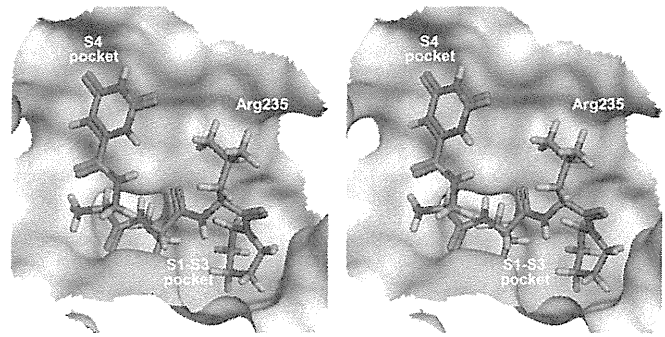

Figure 7. 3D model of inhibitor **54** (KMI1862) docked in BACE1.

Table 3
BAC1 inhibitors with a cyclic amine at the *C*-terminus

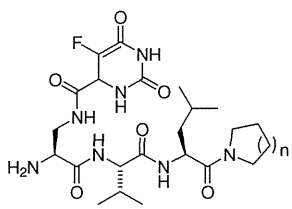

Compound (KMI-No.)	*n*	BACE1 inhibition % at 2 μM
53 (KMI-1861)	1	88
54 (KMI-1862)	2	91
55 (KMI-1802)	3	89
56 (KMI-1803)	4	85
57 (KMI-1804)	5	81

To better understand the observation that inhibitors **3–8** showed potent inhibitory activities, although it lacked a substrate transition-state analogue, a docking simulation study was performed under the MMFF94x force field using MOE software. In examining a docked model of the substrate transition-state of wild-type APP in BACE1 (Fig. 5A), it was apparent that two hydroxyl groups on the substrate's cleavage site interacted with two catalytic Asp side chains. As one oxygen atom of the cleavage site of substrate transition-state derives from water in BACE1, there should be a space corresponding to a water molecule between the substrate and catalytic site. In the docked model of inhibitor 5 (KMI-1565, Fig. 5B), one of two methyl groups at the *C*-terminus of **5** may have bound to the active site by displacing a water molecule in the catalytic site.

Next, tripeptidic BACE1 inhibitors **9–38** were synthesized with modifications at the *C*-terminus (Table 2) and, although most inhibitors with a substituent on the P_1-phenyl ring showed similar inhibitory activities to their corresponding related inhibitors **5–8**, inhibitor **9** with a nitro group on the P_1-phenyl ring and a P_2-Leu residue showed low inhibitory activity. The nitro group of inhibitor **9** might have interacted with the hydrophobic leucine side chain within the molecule. Inhibitor **34** (KMI-1777), with a diiodosubstituted P_1-phenyl ring, exhibited the most potent BACE1 inhibitory activity; the halogen atoms seemed to have enhanced inhibitory activity by interacting with the hydrophobic S_1 pocket.

Based on the finding that the folding configuration around the P_1 phenyl ring of BACE1 inhibitors was important, an inhibitor was envisioned which contained a cyclic amine at its *C*-terminus. As the configurations of some acetyl cyclic amides examined under the MMFF94x force field showed that middle-sized cyclic amides possessed curved structures (Fig. 6A), inhibitors containing a cyclic amine were expected to have a folded configuration (Fig. 6B). Thus, tripeptidic BACE1 inhibitors **53–57** were designed with a cyclic amine at the *C*-terminus (Table 3), and inhibitor **54** (KMI-1862), possessing a six-membered cyclic amine, showed the highest BACE1 inhibitory activity. In the docking simulation model under the MMFF94x force field, inhibitor **54** appeared situated to interact effectively with the BACE1 hydrophobic S_1–S_3 pocket (Fig. 7).

In conclusion, tripeptidic BACE1 inhibitors, designed on the basis of the conformational structure of inhibitors docked in BACE1, revealed the presence of two different types of BACE1 inhibitors, typified by inhibitors **34** (KMI-1777) and **54** (KMI-1862). These inhibitors showed potent inhibitory activities and had lower molecular weights (~500 daltons) than previously reported inhibitors (>600 daltons). Although these tripeptidic BACE1 inhibitors contained some natural amino acid residues, they are expected to have potential as lead compounds for developing the next generation BACE1 inhibitors, because of their low molecular weight.

Acknowledgments

This study was supported in part by the Grants-in-Aid for Scientific Research (A) and (C) from MEXT (Ministry of Education, Culture, Sports, Science and Technology), Japan. (KAKENHI No. 21249007 and No. 23590137, respectively) We thank T. Hamada and Dr. J.-T. Nguyen for performing the in vitro enzyme assays and his help in preparing the manuscript, respectively.

References and notes

1. Selkoe, D. J. *Neuron* **1991**, *6*, 487.
2. Selkoe, D. J. *Nature* **1999**, *399*, A23.